Addis Ababa University
Addis Ababa Institute of Technology
School of Graduate Studies
Energy Center

Simulation of Parabolic Trough Concentrating Solar Power Generation System

By: Seblewongel Tesfu Teferie

A Thesis submitted to the School of Graduate Studies of Addis Ababa University in partial fulfillment of the requirements of the Degree of Masters of Science in Energy Technology

Advisor

Dr.-Ing. Abebayehu Assefa

April 2014

Addis Ababa Institute of Technology
School of Graduate Studies
Energy center

Simulation of Parabolic Trough Concentrating Solar Power Generation System

By: Seblewongel Tesfu Teferie

Approved by the Examining Board:

***Dr.*-Ing. *Abebayehu* Assefa** _____

Chairman, Department's Graduate Committee

***Dr.*-Ing. *Abebayehu* Assefa** _____

Advisor

***Dr. Tesfaye* Dama** _____

External Examiner

***Dr.*-Ing. *Demiss* Alemu** _____

Internal Examiner

Signed Declaration

I declare that the thesis for the M.Sc. degree at the University of Addis Ababa, hereby submitted by me, is my original work and has not previously been submitted for a degree at this or any other university, and that all reference materials contained therein have been duly acknowledged.

Name: Seblewongel Tesfu Teferie

Signature: _____

Abstract

Climate change has drastically increased causing global warming due to emission of greenhouse gas with the provision of energy services that community of the world uses. In order to work against this trend, varieties of researches are necessary to avoid the negative impacts of global warming. Among the various forms, of utilizing energy mechanisms that curtails the emission of greenhouse gases is solar energy electricity production.

In this work, theoretical performance of concentrated solar power system (CSPS) using parabolic trough collectors (PTC) is investigated. The software TRNSYS and the Solar Thermal Electric Components (STEC) library are used to model the power system design and simulations. This model was constructed using data from an existing 30 MW Solar Electric Generating System (SEGS VI) using PTC's in Karmer Junction, California. Input data and results of the simulation of the already existing SEGS VI plant were used for validating the current model.

The validated model is used for building a 10 MW system using TRNSYS. The reference state point properties which are used as inputs in the 10 MW TRNSYS model are determined using MATLAB software. A MATLAB code is used to find the initial pressure after giving first guess for the initial pressure and checking the error. This initial pressure is found to be P (1) = 100 [bar]. This pressure is found for initial steam temperature of 371 ^{O}C. Then, hourly simulations of electrical power and direct normal irradiance (DNI) are determined for selected days of year 2001 (for which complete data are available), for Adigala, Ethiopia.

Different kinds of criteria for land use, annual irradiation and infrastructure are discussed in order to properly locate the CSP plants. Depending on the data gathered and on the criteria set for the CSP installation, north eastern Ethiopia is a suitable site since it has a flat land topology and high solar insolation.

As the cost of power generation by CSP technologies is of great importance for the promotion of the technology to be proven as competitive alternative to the conventional oil or gas fired power plants. This thesis work tackles the economic aspect by investigating the cost of electricity generation of the modeled parabolic trough power plant using simulation tool SAM (System Advisor Model).

Acknowledgment

I would like to thank my advisor Dr.-Ing. Abebayehu Assefa for his support, feedback and encouragement. And also, I am deeply grateful to my family and all of my friends for their everlasting support throughout this thesis work.

Table of Contents

List of Tables

List of Figures

Nomenclature

D	Distance between collector rows
F	Focal length
l	Length of the not irradiated part
L	Length of collector
N	Number of days in years
ST	Solar time
W	Collector aperture

Greek symbols

α_s	surface azimuth angle
$\alpha_{\beta s}^{s}$	sun height
$\tilde{\theta}_z^s$	zenith angle
α	solar altitude angle
β	tilt angle
α_{β}^{δ}	angle of declination
ε	Effectiveness
$\delta_{\varepsilon}^{\varphi}$	Latitude angle
ω	hour angle
θ	incidence angle

Abbreviations

CF	Capacity Factor
CSP	Concentrating Solar Power
DNI	Direct Normal Irradiance
DSG	Direct Steam Generation
EEPCo.	Ethiopian Electric Power Corporation
EHV	Existing High Voltage
EPW	Energy Plus Weather
FWH	Feedwater Heater
GHG	Green House Gas
HCE	Heat Collecting Element
HP	High Pressure
HTF	Heat Transfer Fluid
HV	High Voltage
IDR	Incident Direct Radiation
IEA	International Energy Agency
IPH	Industrial Process Heat
IPP	Independent Power Producer
IR	Interest Rate
IRR	Internal Rate Of Return
LCOE	Levelized Cost Of Electricity
LEC	Levelized Electricity Cost
LP	Low Pressure
NDR	Nominal Discount Rate
NREL	National Renewable Energy Laboratory
NTU	Number Of Transfer Units
PPA	Power Purchase Agreement
PTC	Parabolic Trough Collector
PV	Photovoltaic
RDR	Real Discount Rate
RE	Renewable Energies
SAM	System Advisor Model

SCA	Solar Collector Area
SEGS	Solar Energy Generating Systems
STEC	Solar Thermal Electric Component
SWERA	Solar And Wind Energy Resource Assessment
TRNSYS	Transient System Simulation Program

Chapter 1: Introduction

1.1 Renewable Energy and Climate Change

Energy is a crucial input for technological, industrial, social and economical development of a nation. All societies require energy services to meet basic human needs like lighting, cooking, mobility, communication, etc., but Greenhouse gas (GHG) emissions associated with the provision of energy services can be seen as the major cause of climate change [1].

The earth has warmed by 0.74°C over the last hundred years, and over 50% of this warming has occurred since the 1970s. Global temperatures are likely to rise between 1.1 and 6.4°C (with a best estimate of 1.8 to 4°C) by the end of the 21st century, depending on emissions. This will result in a further rise in global sea levels of between 20cm and 60cm, continued melting of ice caps, glaciers and sea ice, changes in rainfall patterns and intensification of tropical cyclones. Food shortages and the spread of disease are commonly predicted.

At present, just over 7 billion tonnes of CO_2 is emitted globally each year through fossil fuel use. The concentrations of these gases in the atmosphere have now reached levels unprecedented for tens of thousands of years.

Renewable energies (RE) offer a great chance in reducing the GHG emissions in an economical way. The costs and the challenges for the integration of RE into an existing energy supply system is mainly dependent on the actual system characteristic, the current share of RE and the availability of RE resources. Countries in transition and developing countries have more time to reduce their emissions. However, taking into consideration the growth of population and the ongoing development in countries of transition and developing countries, a significant increase in energy consumption along with GHG emissions will be noticed.

Ethiopia is one of the countries where significant increase in energy consumption has been experienced recently. Electricity sales increased from 3,131.26 GWh in 2008 to 3,264.42 GWh in 2009 by 4.25 % [2]. Therefore, to compensate the increase in demand and to mitigate climate change, different energy potentials should be explored.

1.2 Energy Potential of Ethiopia

In Ethiopia, substantial renewable energy resources do exist consisting mainly, hydropower, wind, geothermal, biomass and solar energy. The country also has considerable non-renewable energy resources especially natural gas and coal. The energy sector is currently dominated by traditional biomass consumption, other energy sources such as hydropower and the rest renewable energy resources can potentially offer the nation for major economic development opportunities.

1.3 Solar Energy Potential

Solar energy is clean, unlimited and safe. Even when it is converted into electricity through photovoltaic or thermodynamic plants, it does not produce harmful emissions. That is why this renewable energy source has assumed a key role in the future of energy policy. Many governments started incentive plans to promote generation and integration of energy into the grid by means that minimize the environmental impact.

Ethiopia has substantial solar energy resource. However, less than 1% of the potential has been exploited so far. According to the recent data collected by energy information administration and development follow up core process, within the last 6 years, the total generated energy from solar photovoltaic is more than 35 MWh, more than 6MW than the installed capacity. Solar water heating systems with the total energy generation of 299 MWh and ten water pumps with pumping installed capacity of 10 kW have been installed in different parts of the country by governmental and nongovernmental organizations [3].

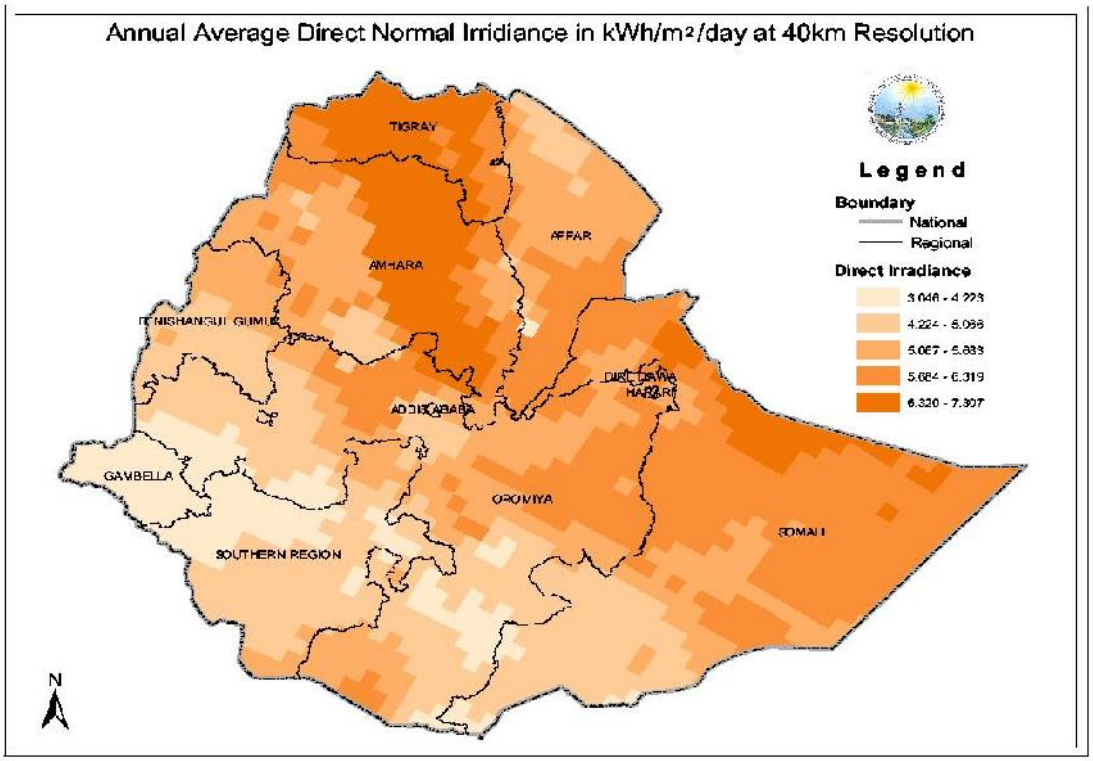

Figure 1.1: Solar energy generation potential

1.4 Solar Technology

Solar technology, for power generation, can be broadly classified into photovoltaic (PV) and concentrating solar power (CSP). In PV technologies, semiconductor materials are used in solar panels to convert photons in sunlight directly to electricity. Whereas, CSP technologies are those that concentrate the sun's energy to heat a working fluid (liquid, solid or gas) and then used in a downstream process for electricity generation. A more economical method is using concentrating solar power (CSP) technologies to meet a significant portion of the future energy demands in an environmentally clean and cost-effective way. And also CSP technology is a superb and a viable option as it is not sensitive to drought or to fuel price fluctuations while it relies upon a secure and local resource: the Sun.

Key factor that affects the CSP plant size, performance and land occupation, is the direct normal irradiation of selected site. United Nations Environment Program study revealed that a minimum

threshold value of 1,800 kWh/m^2/ year of direct normal irradiance (DNI) as a prerequisite for CSP installations [http://www.hgcoc.com].

In this project, further development of Ethiopia's research capacity in alternative energy systems with particular emphasis on parabolic trough solar power generation is considered. In doing so, a particular site called Adigala, which is found in the province of Somalia in Ethiopia located at latitude 10.41^o and longitude 42.21^o with an annual averaged direct normal radiation of 6.68 (kWh/m^2/day) [4] is chosen for a power plant simulation capacity of 10 MWe.

1.5 Objectives of the Thesis

This thesis has the following objectives

- Investigating solar radiation data of Adigala to come up with a model of concentrated solar power plant system;
- Investigating the criteria for land use, annual irradiation and infrastructure for weather prediction; and
- Investigating the economical viability of the system designed.

1.6 Literature Review

Around 1883, Captain John Ericsson used a longitudinal parabolic concentrator to operate on solar-powered machine intended for irrigation purposes. His experiments with solar engines never advanced beyond the prototype stage.

It is indeed a pity that Ericsson had a somewhat eccentric attachment to secrecy regarding his research, given that he died in 1889 with no record of the extent of his progress on what was reputed to be a much more advanced solar motor [http://www.bicyclecity.com].

Even so, the invention of the parabolic trough is significant. In 1912, it enabled the construction of a 45kW power generation plant in Meadi, Egypt. The system consisted of five collectors oriented in a north-south direction with a mechanical tracking system. Each collector was 62m in length and 4m in width with spacing of 7.6m [6]. The system generated steam that was used to power water pump for irrigation purposes. The system is shown in Figure 1.2:

Figure 1.2: Shuman-Boys solar power plant, Egypt, 1913.

Sadly, a combination of the advent of First World War and declining interest in alternative energy due to lower fossil fuel prices forced the plant to close down. The demise of the Meadi Plant did not mean the end of the parabolic trough. This invention, in its modernized form, survived and spawned the growth of alternative energy industry. Luz Co. immediately comes to mind, as an example of a company that took the initiative to see where this technology might lead.

Recent development of parabolic trough power plants took place in the U.S. in mid-1970s and in Europe in 1980s [7].Parabolic trough collectors capable of generating temperatures greater than 500ºC were initially developed for Industrial Process Heat (IPH) applications. Much of the early development was conducted by or sponsored through Sandia National Laboratories in New Mexico.

The development was terminated with the construction of the International Energy Agency (IEA) Small Solar Power Systems Project/Distributed Collector System in Tabernas, Spain, in 1981. This facility consisted of two parabolic trough solar fields with a total mirror aperture area of 7602 m^2. The fields used the single-axis tracking Acurex collectors and the double-axis tracking parabolic trough collectors developed by M.A.N. of Munich, Germany.

In 1982, Luz International Limited (Luz) developed a parabolic trough collector. Starting in 1985, Luz built eight parabolic trough power plants in California, in the US.

Table 1.1: Thermal solar collector assemblies, SCAs characteristics

Collector	**Acurex**	**MAN M480**	**Luz LS-1**	**Luz LS-2**		**Luz LS-3**
Year	1981	1984	1984	1985	1988	1989
Area [m^2]	34	850	128	235		545
Aperture [m]	1.8	2.4	2.5	5		5.7
Length [m]	20	3	50	48		99
Receiver diameter[m]	0.051	0.058	0.042	0.07		0.07
Concentration ratio	36:1	41:1	61:1	71:1		82:1
Optical efficiency	0.77	0.77	0.734	0.737	0.764	0.8
Receiver absorptivity	0.96	0.96	0.94	0.94	0.99	0.96
Mirror reflectivity	0.93	0.93	0.94	0.94	0.94	0.94
Receiver emittance @ temperature [^oC]	0.27	0.17	0.3 300	0.24 300	0.19 350	0.19 350
Operating temp. [^oC]	295	307	307	349	390	390

Table 1.2: Characteristics of Solar Electric Generating Systems SEGS I through IX [8]

SEGS Plant	**1st Year of Operation**	**Net Output [MWe]**	**Solar Field Outlet Temp. [^oC]**	**Solar Field Area [m^2]**	**Solar Turbine Eff. [%]**	**Fossil Turbine Eff. [%]**	**Annual Output [MWh]**
I	1985	13.8	307	82,960	31.5	-	30,100
II	1986	30	316	190,338	29.4	37.3	80,500
III/IV	1987	30	349	230,300	30.6	37.4	92,780
V	1988	30	349	250,500	30.6	37.4	91,820
VI	1989	30	390	188,000	37.5	39.5	90,850
VII	1989	30	390	194,280	37.5	39.5	92,646
VIII	1990	80	390	464,340	37.6	37.6	252,750
IX	1991	80	390	483,960	37.6	37.6	256,125

The plants are designed to produce full electrical power with steam supplied either by solar field or by natural gas (via the gas-fired boiler).

There are other operational parabolic trough power plants in the US such as Nevada Solar One plant with 72 MWe net capacity and Martin Next Generation Solar Energy Center plant with a net capacity of 75 MWe.

Coming to the continent Europe, the first parabolic trough power plant is Andasol 1 which is in Spain. The construction of the plant started in 2006 and the power production began in November 2008. Andasol 1 is the first parabolic trough power plant with storage system where 7.5 hours storage system is integrated in the plant.

There are many other plants in Spain of similar characteristics either operational such as Anadasol 2 (50 MW with 7.5h storage) and Majadas 1 (50 MW with storage), or under construction like Vallesol 50 (50 MW with 7.5h storage) [9].

Up to now scholars tried and are still trying to investigate and model existing parabolic trough power plants performance in order to improve their efficiency so that future intended parabolic trough power plant design improves.

As a result, a typical 30 MWe SEGS plant was studied using a detailed thermodynamic model by Lippke [10]. In this model, correlations for the performance of parabolic trough solar collectors were derived based on measured data under different conditions; these correlations were used to calculate the energy obtained from the solar field. The model was used to calculate the gross and net electricity output under different operating conditions. A comparison was made of the model results to real plant conditions for a winter and summer day in order to test the accuracy of the model and shows that the model still lacks the capability to fully account for actual solar field conditions.

A detailed performance model of the 30 MWe SEGS VI parabolic trough plant in TRNSYS was created. This model included solar and power cycle performance without fossil backup. The model was created to accurately predict the SEGS VI plant behavior and to examine transient effects such as start up, shutdown, and system response. Good agreement between model predictions and plant measurements was found, with errors usually less than 10%, and transient

effects such as startup, shutdown, and cloud response were adequately modeled. While the model could be improved, it demonstrates the capability to perform detailed analysis and is useful for such things as evaluating proposed trough storage systems [11].

A methodology was presented for economic optimization of solar plant design as a function of the solar irradiance in 2002[12]. This model was able to find the optimal solar field size for any specific project location.

Another simulation [13] for the solar field based on SEGS VI was modeled in TRNSYS. In this simulation, the Rankine power cycle was separately modeled; the steady-state power cycle performance was regressed in terms of the heat transfer fluid temperature, heat transfer fluid mass flow rate, and condensing pressure, and implemented in TRNSYS. Both the solar field and power cycle models were validated with measured temperature and flow rate data from the SEGS VI plant.

As a result, parabolic trough concentrating system can be used as an alternative electric generation for Ethiopia using the sun as a fuel with the existing Ethiopian grid system.

1.7 Methodology

After conducting relevant materials review on parabolic trough collectors and power production from steam using Rankine cycle, the SEGS VI plant was chosen for modeling the intended model for Ethiopia because it has been well characterized and there exists data from other researches. The methodology held here is modeling the SEGS VI plant and validating it using the same data as the plant. After that, by reducing number of turbine and feedwater heaters, 10 MW plant is intended to be modeled.

1.7.1 Data Collection

Considering numerous criteria such as ground structure, water bodies, slope, protected and/or restricted areas, forest, and agricultural covered areas for the detection of land resources, which would permit the placement of concentrating solar collector fields, data has been collected in map format. These data sets are combined in order to yield a usable area. Weather data is also taken from SWERA and National Solar Radiation Data Base (USA) for simulation of model.

1.7.2 Analysis

To accomplish the desired objectives, reviewing literatures and other resources which are relevant to this thesis work are followed. TRNSYS software is used to model the power plant using STEC (Solar Thermal Electric Components), TRNSYS library. TRNSYS is software which is developed primarily at the University of Wisconsin and is a complete and extensible simulation environment for the transient simulation of systems. Models of individual components called Types can be created. These models of individual components are then connected within TRNSYS and simulations for the larger system are run. Each Type of component is described by a mathematical model in the TRNSYS simulation engine.

MATLAB modeling of the power plant is used to find different state reference values (pressure, steam temperature, enthalpy) which are used as inputs for the TRNSYS modeling and simulation of the power plant.

The economical analysis of the project is prepared using software called Solar Adviser Model (SAM). SAM is a performance and financial model designed to facilitate decision making for people involved in the renewable energy industry such as project managers and engineers, policy analysts, technology developers and researchers. SAM makes performance predictions and cost of energy estimates for grid-connected power projects based on installation and operating costs and system design parameters that the user specify as inputs to the model.

Chapter 2: Concentrated Solar Power Technology

Concentrating solar power (CSP) technologies produce electricity by concentrating direct-beam solar irradiance to heat a liquid, solid or gas that is then used in a downstream process for electricity generation. Majority of the world's electricity production nowadays derives from nuclear, coal, gas, oil and biomass driven power plants. The CSP plants work on the same concept while providing an alternative heat source. Therefore, CSP can benefit from not only the improvements made in the solar concentrator technologies but also from the ongoing advantages in steam and gas turbine cycles.

From other forms of renewable, CSPs are unique in that they have the option to incorporate thermal storage to store solar-generated energy for use at a later time in their design making power from CSP plants dispatchable. Thus, CSP offers firm, flexible electrical production capacity to utilities and grid operators while enabling effective management of a greater share of variable energy from other renewable sources (e.g. photovoltaic and wind power).

Parabolic trough, linear Fresnel reflector, power tower, and dish engine technologies fall into the CSP category. In all of these systems, a working fluid is heated by the concentrated sunlight and is then used for power generation or energy storage.
Some of the key advantages of CSP include the following [14]:

- It can be installed in a range of capacities to suit varying applications and conditions, from tens of kW (dish/Stirling systems) to multiple MWs (tower and trough systems);
- It can integrate thermal storage for peak loads (less than one hour) and intermediate loads (three to six hours) for operations on grid stability;
- It has modular and scalable components; and
- It does not require exotic materials.

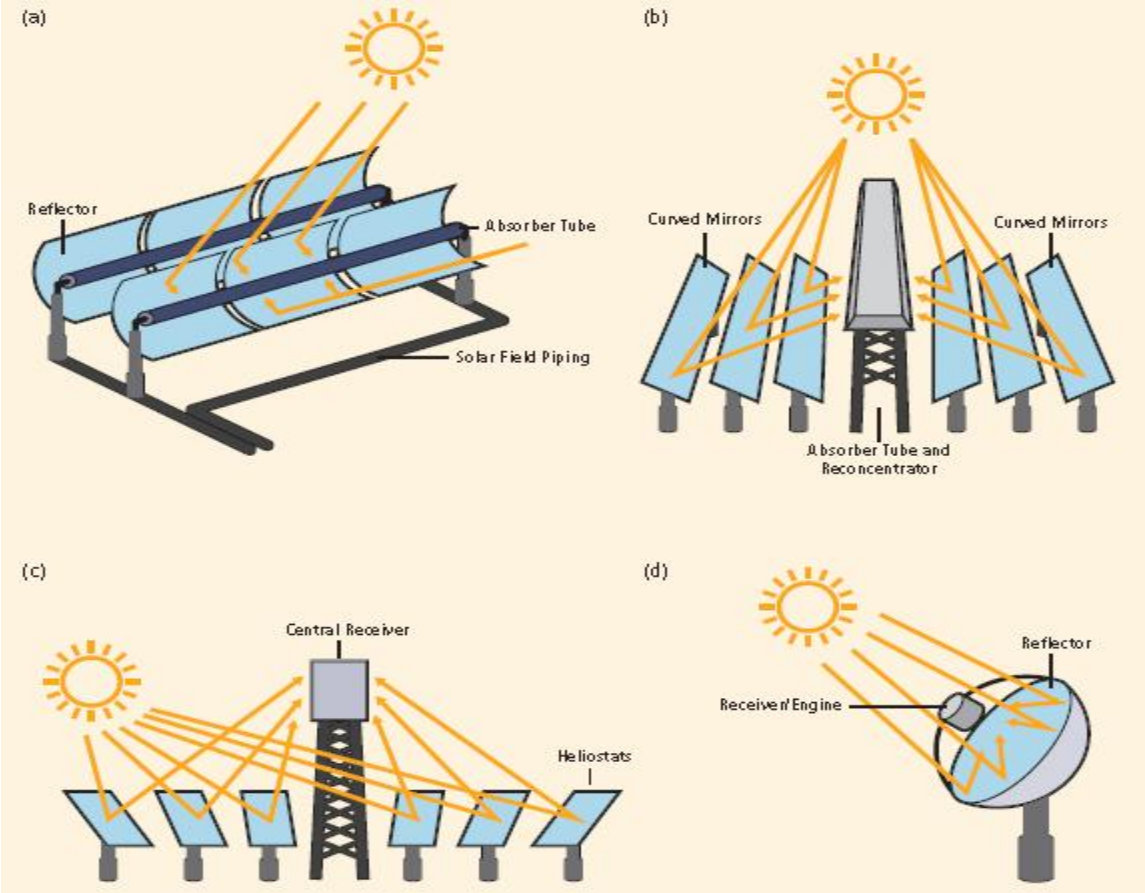

Figure 2.1: Schematic diagrams of CSP configurations: (a) Parabolic trough, (b) Linear Fresnel reflector, (c) Central receiver/power tower, and (d) Dish systems (Richter et al., 2009)

The Solar Electricity Generating Systems (SEGS), in the southwest desert of California [15] where DNI is quite favorable for CSP, shows impressive cost reductions as shown in Figure 2.2. These parabolic trough plants have been operating successfully for over three decades, thus providing valuable data. As indicated in the Figure, the advanced concepts, with large-scale implementation and improved plant operation and maintenance, provide a great opportunity for further reductions in the levelized electricity cost (LEC). Life cycle assessment of emissions and land surface impacts of the CSP systems suggest that they are best suited for greenhouse gas and other pollutant reductions. CSP systems are also best suited, because of the effortless capture of

the waste heat, for multi generation applications, such as the simultaneous production of electricity and water purification which will not be discussed in this thesis Project.

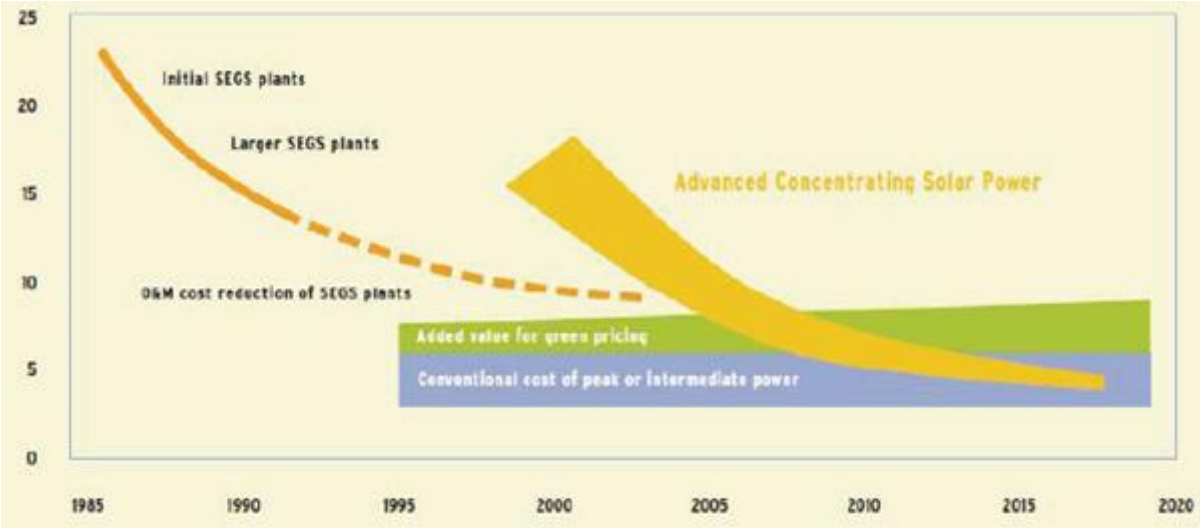

Figure 2.2: Levelized electricity cost (cents/kWh) projections of CSP (Source: Solar Paces)

Because of rapid developments occurring, both in technology and electricity market strategies, CSP has the greatest potential of any single renewable energy area. It also has significant potential for further development and achieving low cost because of its guaranteed fuel supply the Sun.

2.1 Technical Factors in CSP

2.1.1 Landscape Impact

The CSP plant's land occupation depends on the total installed collector surface and also on the space between each solar collector assembly required to minimize shadows and also to allow the maintenance of the big curved reflecting mirrors. Additional surface is also required for the power block, usually located in the middle of the plant an area much smaller with respect to the solar field.

The solar field area of each plant, in a determinate location with a certain daily average direct normal irradiation, needs to be optimized with respect to solar collector area in order to reach the minimum levelized cost of energy.

2.1.2 Performance

Performance of a CSP plant is affected by variations in solar radiation, characteristics of solar collectors, and by geometrical factors such as shadows.

An efficiency factor called “capacity factor (CF)” of the plant exists for CSP. This is the ratio of the energy produced by the plant over the course of the year to the output the system operated at its name plate capacity (e.g. nominal size of the steam turbine for 8760 hours).

The capacity factor strongly depends on the solar resource available in a certain location and on the solar field size, so on the area of the mirrors. Oversized solar field allows the plant to provide more thermal energy to the power block and consequently results in a higher capacity factor but also leads to an increase of investment cost. On the other hand, if the solar field area is reduced, a consistent part of the potentially available solar energy is dumped during high solar radiation days: the thermal energy to the power block is beyond the steam turbine maximum admissible thermal input.

2.1.3 Interaction of CSP with the Grid

Large-scale integration of multi megawatt solar plants, especially utility scale PV plants, into grid operation would lead to new operation constraints (e.g. power is produced during the day, when the electricity demand is high, thus it is valuable peak current), for the entire high voltage (HV) distribution and transmission system, that could result unacceptable in the next years in terms of system performance (grid and generating plant).

In terms of grid impact, CSP generation is highly predictable since any CSP plant is intrinsically coupled with thermal storage which enables the CSP plant to easily meet the load demand curve at any time, day and first hours of night time, and can cover peak hours demand if they are scheduled. Furthermore CSP plants can easily participate to primary and secondary grid

frequency control so that they are able to support grid exploitation both during steady state and transient condition.

The growth of utility scaled plant is granted only if unlimited access to the HV and extra high voltage (EHV) grid is allowed. Besides this issue, the higher penetration of renewable energies (especially wind and solar) harbors the risk of grid instability in case the generating plants not able to properly support the grid. This leads to the search for new developments with respect to the device design which should be armed with the task of supporting the grid operation and stability.

Among CSP technologies, parabolic trough power plant technology has been in use for over three decades. This is currently the cheapest and most proven technology for commercial solar thermal power generation.

2.2 Parabolic Trough Technology

A parabolic trough power generation uses parabolic mirrors that line up in long rows to concentrate sun light onto an absorber tube (receiver). The receiver contains a heat transfer fluid (the simplest being mineral oils used in early plants, eutectic fluids, and the most challenging molten salts) that is heated and circulated, and the heat is released to generate steam. The steam powers a conventional steam generator to produce electricity. The mirrors use a single-axis tracker to ensure that the sun is continuously focused on the receiver requiring a fairly flat land. A simple schematic, shown in Figure 2.3, describes the main elements of such a system.

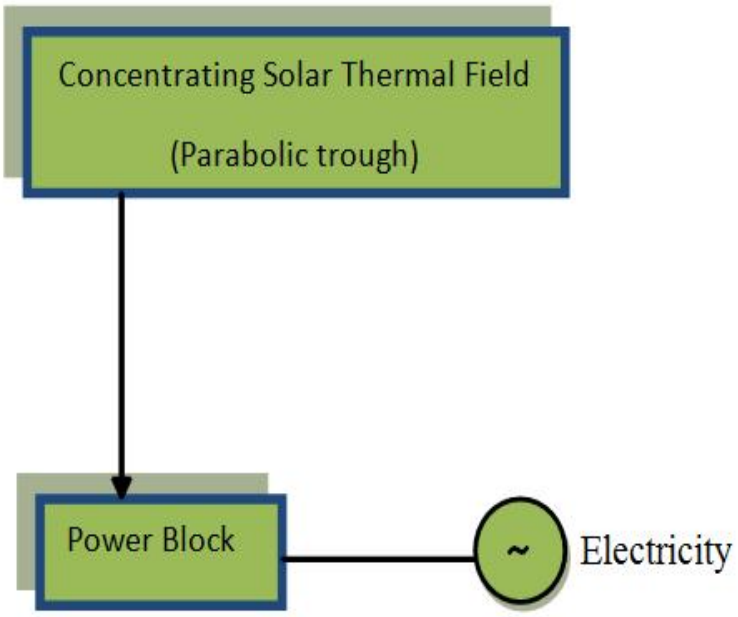

Figure 2.3: Main components of parabolic CSP system

In this technology the solar field is composed of glass mirrors of parabolic shape which reflects direct normal radiation. The complete construction is a lightweight metal structure, which normally is equipped with a single axis tracking system.

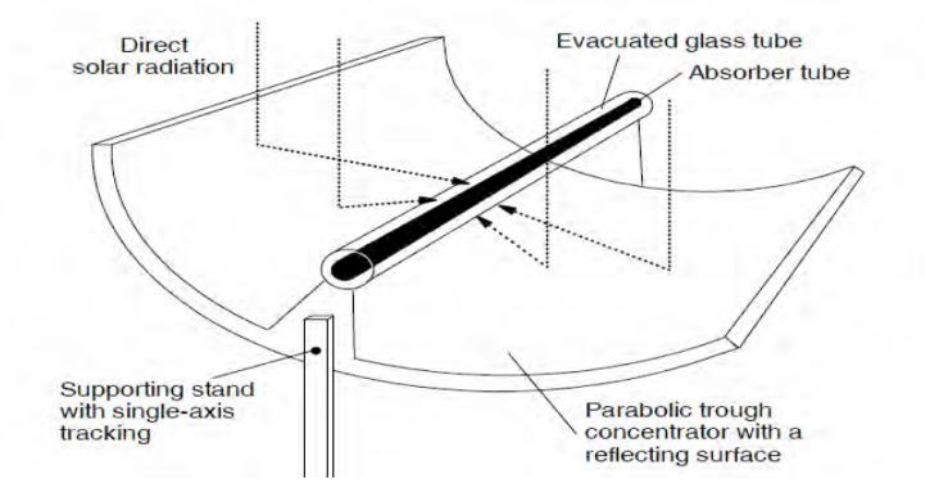

Figure 2.4: Functional principle of a parabolic trough

A complete solar field contains several parallel rows of solar collectors. The distance between the collector rows is planned according to minimizing the piping costs on the one hand and having a minimal shading effect between the rows on the other. In general, the design of the solar field depends on plant and collector size, the temperature and pressure losses in the piping system and the specific ambient conditions. Parabolic trough fields can be erected in any direction, but erected in a north-south direction leads to the highest possible energy yield over the year while an east-west orientation smoothes down the seasonal fluctuations.

Some of the components like the metal structure, the tracking system, the controllers and other subsystems, which make up around 60% of the direct solar field costs, are standard components and can be ordered from several countries and in different forms. The reflectors and the absorber tube, however, are special components and have to be produced specifically for the parabolic trough solar field.

2.2.1 Reflectors

The concentrators, Figure2.4, consist of a heat-formed glass cake. It is carried by the metal structure of the collector. Glass, which is used in solar applications, must have very low iron content for getting a transmissivity in the solar spectrum of around 90%.

2.2.2 Absorber

For parabolic trough collectors, the absorber pipe consists of a tube. A glass pipe surrounds the tube Figure 2.5. The glass tube allows evacuating of the area between the absorber tube and the glass pipe in order to minimize convection and conduction heat losses.

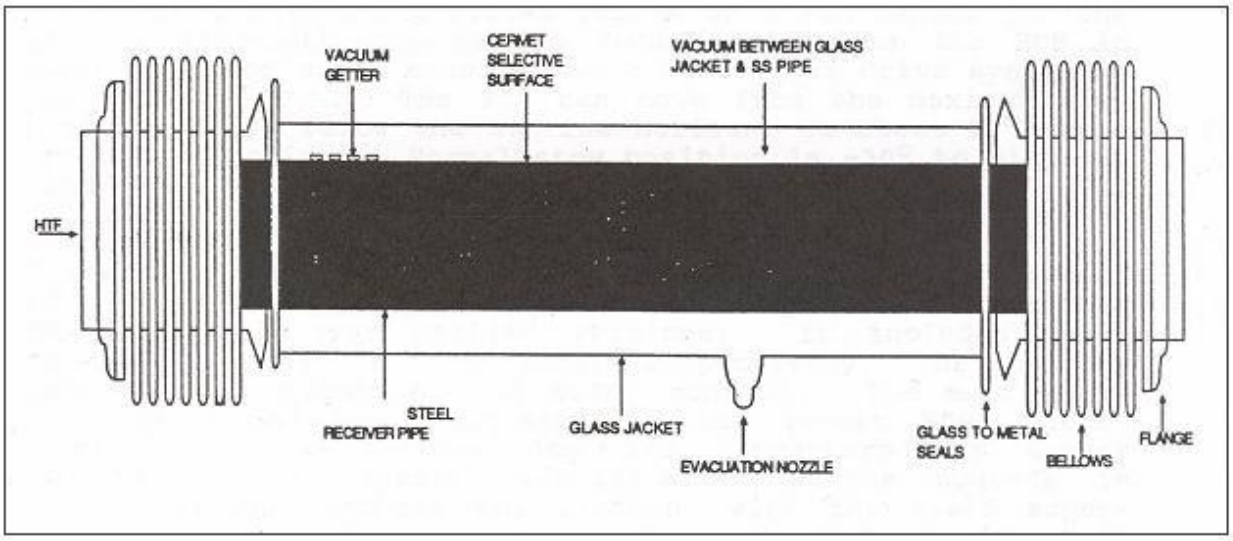

Figure 2.5: Absorber tube of a parabolic trough collector

Vacuum tubes should be designed using the most suitable material and geometry to absorb the maximum amount of solar energy. Vacuum tubes are usually formed using a cermet coated stainless steel absorber tube surrounded by a glass envelope. The outer glass tube is transparent to shortwave radiation and allows light rays to pass through with minimal reflection. The inner tube is coated with a special selective coating. The coated absorber layer should have high radiative absorbtivity at short wavelengths and low radiative emissivity at long wavelengths. The air between the two tubes is removed making vacuum.

2.2.3 Tracking and Controlling

Solar fields in a CSP plant use single axis tracking systems. The tracking is according to the position of the sun and/or the requirement of the power block. Therefore a solar sensor is used to evaluate the sun position. Sensors consisting of a convex lens focus the sun light to a small photovoltaic cell, reaching a resolution of around 0.05%. These kinds of sensors are used in the so-called SEGS plants, where they prove most effective. The tracking system must have sufficient torque to operate the collectors even at higher wind speeds.

In existing plants, the controlling of the field takes place in two separate stages. The overall control is located in the central control room and the second stage is placed on each collector unit. The local units take care of the incoming irradiation, wind speed and mass flow of heat transport medium. In case of emergency the local units can shut down parts of the solar field.

The overall unit operates the solar field according to the overall plant requirements, mainly the electrical output in relation to the actual solar radiation.

2.2.4 Heat Transfer Medium

At the moment high-boiling synthetic thermal oil are being used as the heat transfer medium in the absorber tubes. According to the thermal stability of this oil, the actual operation temperature of the solar field is approximately 400°C. When operating at this temperature, the oil has to be pressurized at around 12 to 16 bar. The thermal oil is circulating in the collector tubes, where the driving forces are speed adjustable pumps. For the purpose of thermal expansion during its heat up an expansion vessel is installed.

Chapter 3: Considerations in Assessment for CSP

3.1 General Description of Selected Site

In Ethiopia there are different sites which have rich solar potential. Among these the Somalia region is one of them. Somalia region is divided into Woredas. Shinle Woreda is one of them; it consists of different kinds of land topology but mostly flat lands. In this Woreda, a place called Adigala is chosen for this particular study. Geographically, the system's site is located at latitude 10.41^{o} and longitude 42.21^{o} with an annual averaged direct normal radiation of 6.68 ($kWh/m^2/day$). A substation also exists at this place for Ethio-Djibouti power transmission which will be required for CSP production. In order to select this particular site, different considerations were taken.

3.2 Land

To identify major locations for CSP installation, land assessment has to be considered. Areas with $<1km^2$ should be eliminated. Thus assessment criteria are required. Some of criteria that will be used can be seen as optional. For instance, tourist areas or agricultural areas can be transformed into potential sites for CSP plants. Other information like slope of the terrain or water availability can be understood as necessary criteria. For example if the slope of the terrain is greater than 2.1% the placement of a CSP plant will be impossible, considering the state of the current technologies, impossible. Table 3.1 lists the necessary and optional criteria.

Table 3.1: Necessary and optional criteria an area must fulfill for being considered as a possible construction site for a CSP plant

Excluded criteria	Necessary	Optional
Slope of terrain		
>2.1%	X	
Land cover		
Inland water	X	
Forest		X
Swamp	X	
Agriculture		X
Hydrology		
Permanent inland water	X	
Non- permanent inlet water		X
Regularly Flood area		X
Geomorphology		
Shifting sand, dune	X	
Security Zone for Shifting Sands 10km		X
Salt pans		X
Land use		
Settlements		X
Airport		X
Oil gas fields		X
Mine, quarry		X
Protected area		X
Restricted area		X

As shown in Figure 3.1 (center of Adigala), contour lines are further apart indicating the gradient is flatter. Therefore, the further apart they are located, the flatter the ground gets. At the site a

well exists. There are no swamps or drifting sands. Therefore the site is excellent for CSP installation given the criteria listed in Table 3.1.

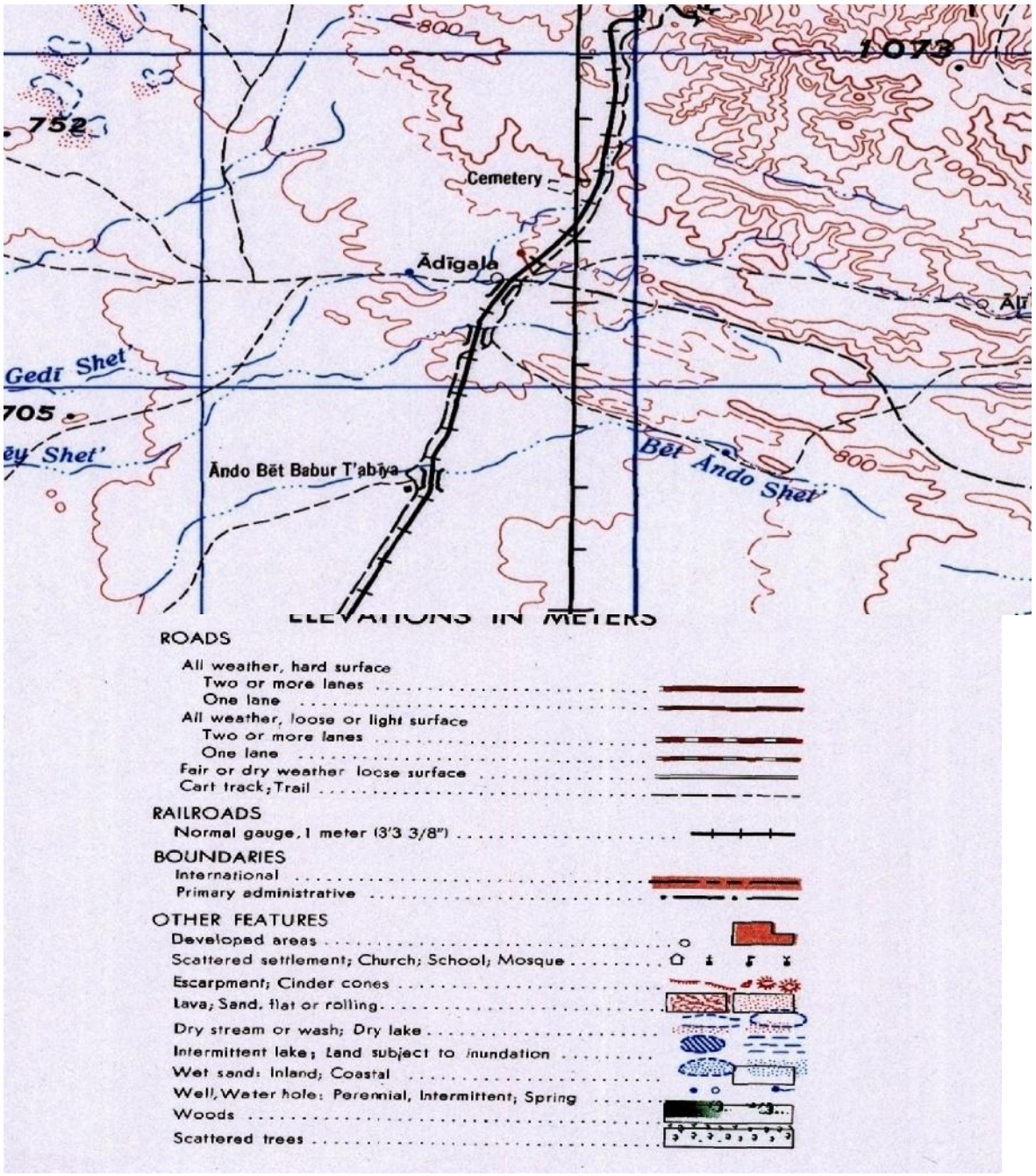

Figure 3.1: Portion of map representing Adigala

Source: Ethiopian Map Agency

3.2.1 Geomorphologic Features

For CSP project flat land is requirement. As can be seen from the Figure the geomorphologic features of the land of north eastern Ethiopia, which is marked in red star, is suitable for CSP installation considering plain surface of area.

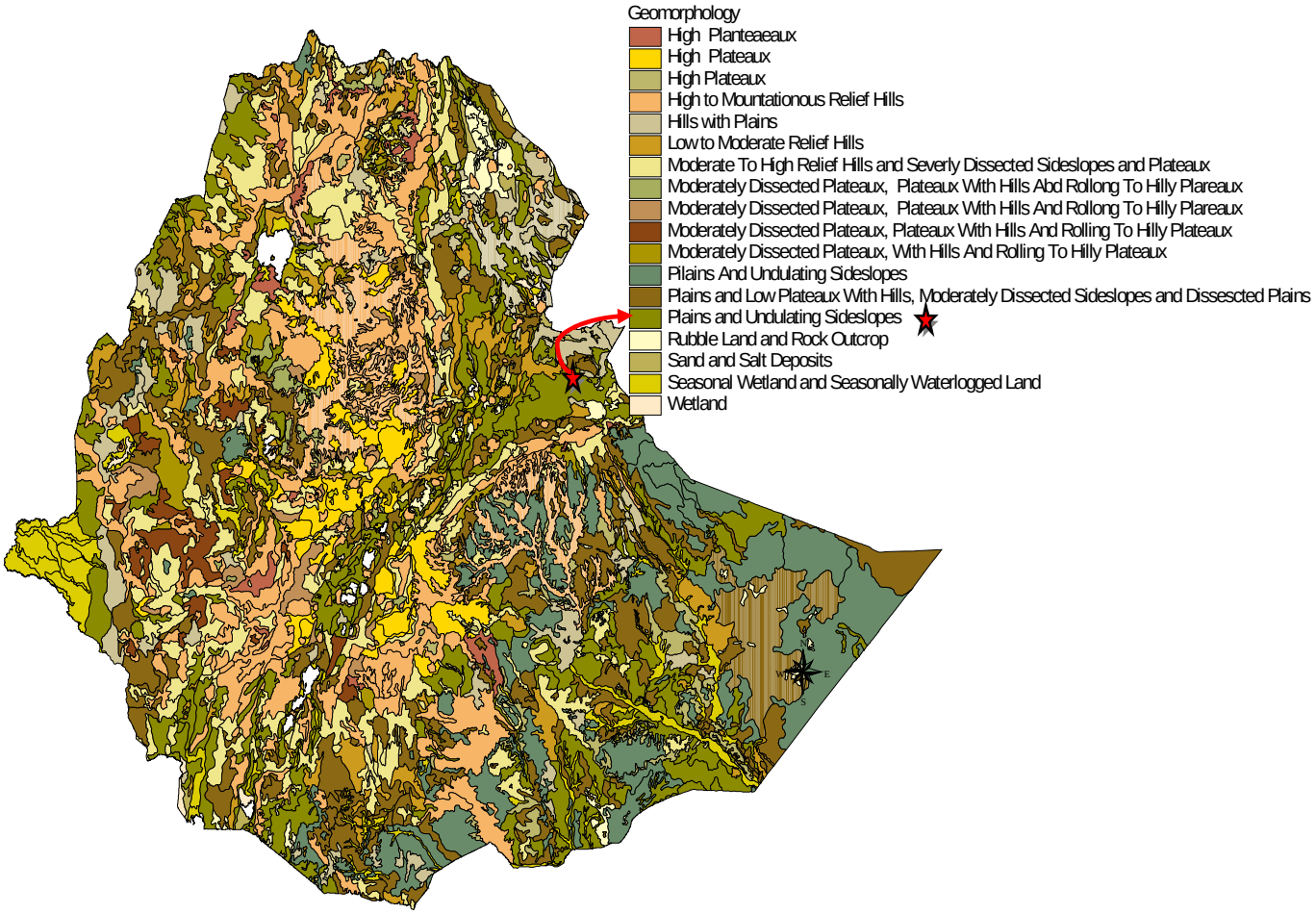

Figure 3.2: Geomorphologic features of Ethiopia

3.2.2 Technical Potential

A site is considered to have a technical potential for a CSP plant when the yearly average direct irradiation is 1800 kWh/m^2/year and above. Taking into consideration economical factors, CSP starts to become feasible with a higher irradiation. And, the selected site yearly average direct irradiation qualifies a suitable value for operating a CSP plant.

3.2.3 High Voltage Grid

In order to supply the electrical energy produced by CSP plant, a connection point to the transmission grid is required. In this work, only the actual existing high voltage and extra high voltage grid systems are taken into consideration.

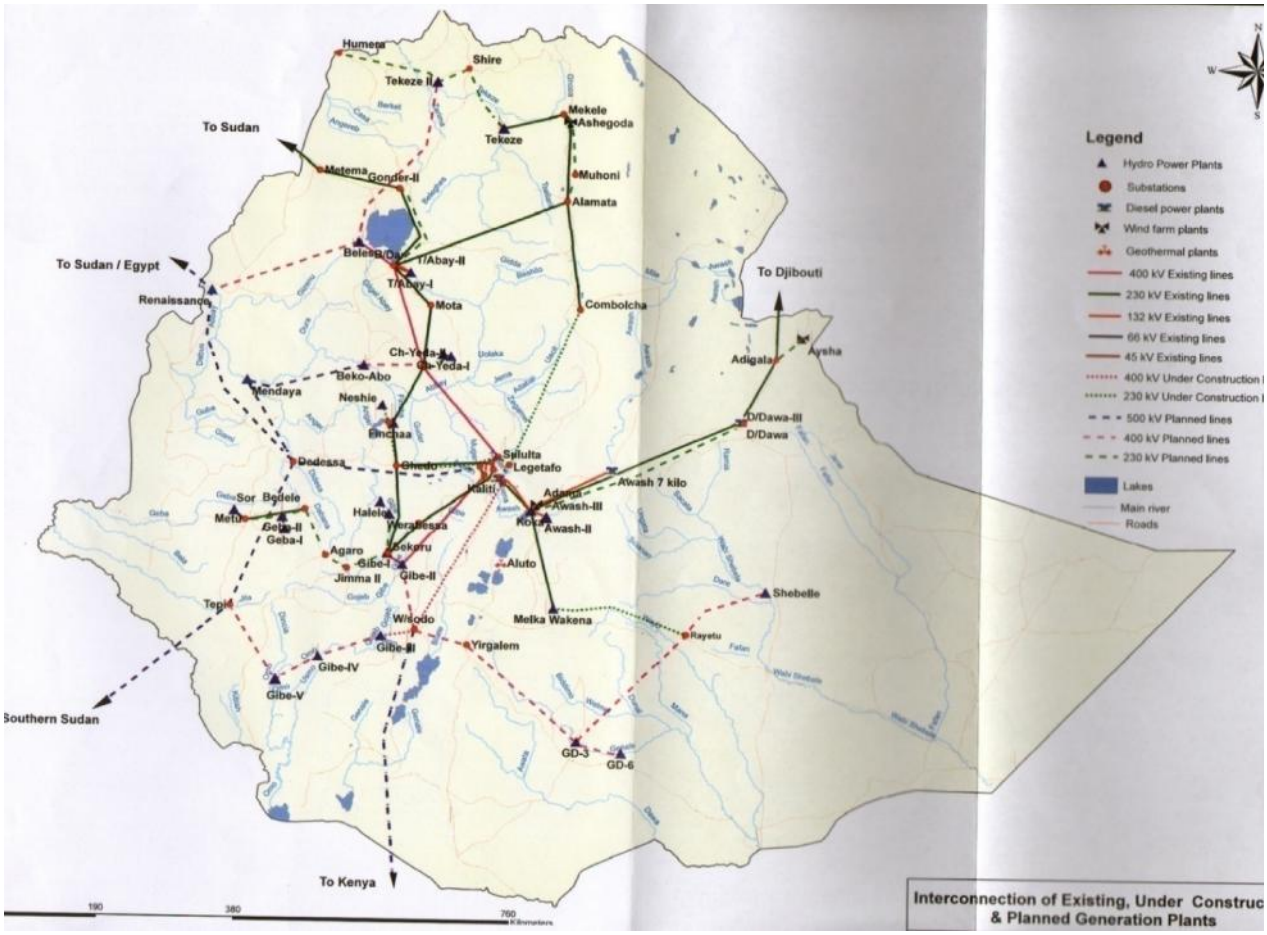

Figure 3.3: Interconnection of existing transmission grid and substations for Ethiopia

Chapter 4: Theoretical Performance Calculation of CSP

Incoming radiation from the sun is direct normal radiation, which is absorbed by collector of a solar field, used as a fuel for a CSP plant. For a precise calculation of the CSP plant performance it is needed to understand the geometrical relations between the sun and earth at any time of the day. In this chapter, these theoretical relations are described.

4.1 Sun Earth Geometry

The geometrical relationship between the incoming direct radiation and a plane of any orientation at every hour can be described in terms of several angles. The following schematic drawing gives an overview of these geometrical relations.

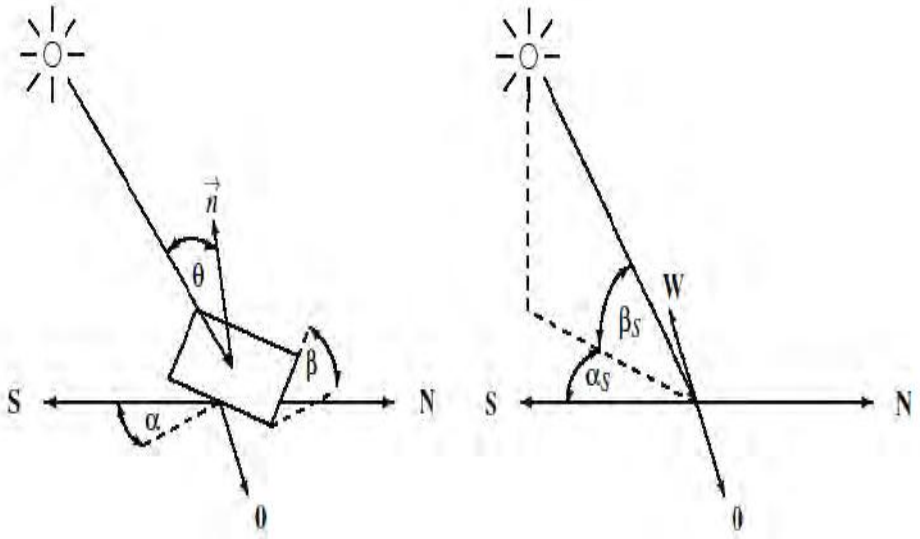

Figure 4.1: Geometrical relation between sunbeam and tilted surface

The most important angel, in this arrangement is the so-called incidence angleθ, and it can be calculated from:

$$\cos\theta = \sin\delta\sin\phi\cos\beta - \sin\delta\cos\phi\sin\beta\cos\alpha + \cos\delta\cos\phi\cos\beta\cos\omega + \cos\delta\sin\phi\sin\beta\cos\alpha\cos\omega + \cos\delta\sin\beta\sin\alpha\sin\omega \quad (4.1)$$

where:

β - is the tilt angle of the plane,

ω - is the hour angle and it describes the earth's rotation about its polar axis,

α - is surface azimuth angle, with 0 in the southern direction, if negative moving towards an eastern direction or positive in a western direction. Both β and α angles can be adjusted or fixed using tracking system according to the suns position;

ϕ - is latitude angle and

δ - is angle of declination and can be approximated by the equation of cooper (1969) where N is number of days in years.

The plane that includes the earth's equator is called the equatorial plane. If a line is drawn between the center of the earth and the sun, it is the angle between this line and the earth's equatorial plane is called the Declination angle δ.

$$\delta = 23.45\, sin\left(360\frac{284+N}{365}\right) \tag{4.2}$$

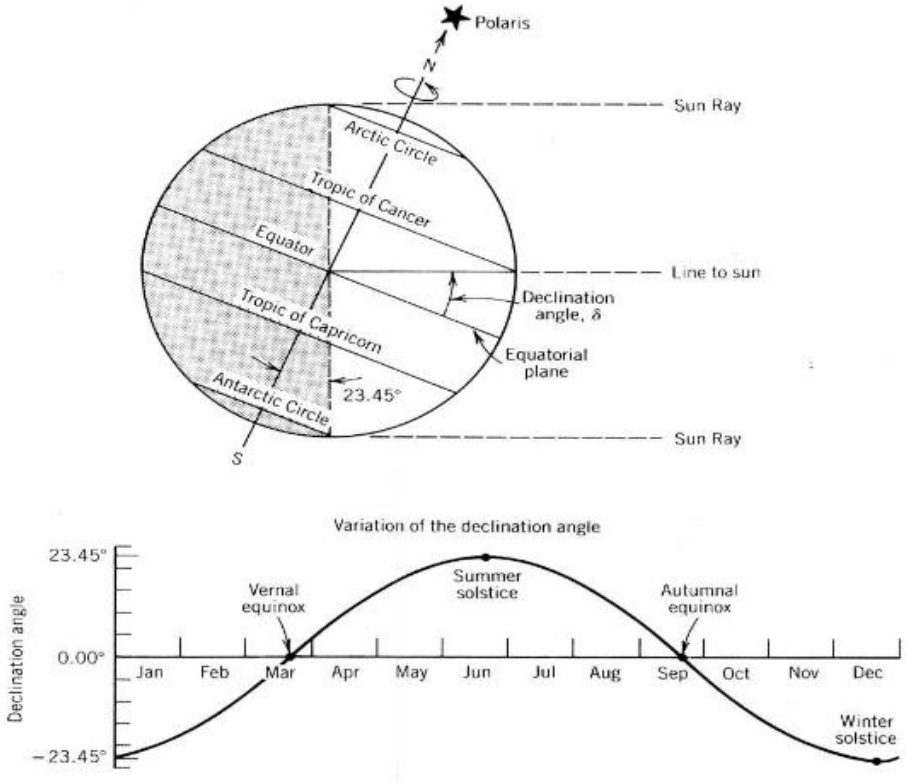

Figure 4.2: Declination angle

The hour angle describes the earth's rotation about its polar axis whether the sun is east or west of the local meridian. This is done due to rotation of the earth with a value of around 15° per hour. The hour angle is zero at solar noon (when the sun reaches its highest point in the sky). The hour angle increases by 15^{o} and solar time ST in hours are related as:

$$\omega = (ST - 12)x15^{c} \tag{4.3}$$

The angle will be negative in the morning and positive in the afternoon.

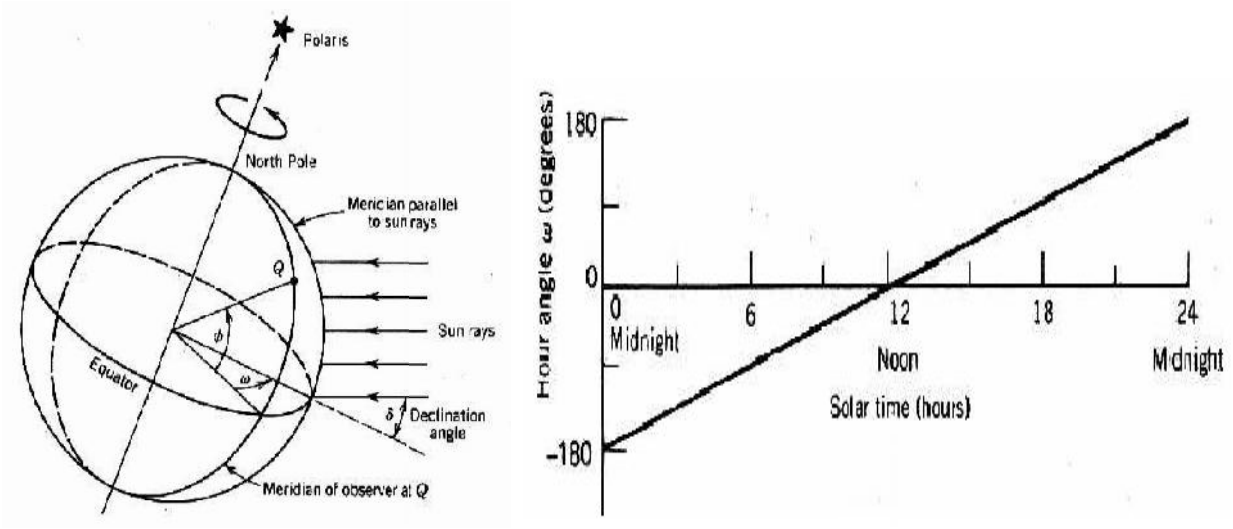

Figure 4.3: (a) Hour angle (b) Hour angle (ω) variation in a day

The zenith angle can be understood as the incidence angle of beam radiation on a horizontal surface.

$$cos\,\theta_z = (cos\,\emptyset\,cos\,\delta\,cos\,\omega + sin\,\emptyset\,sin\,\delta) \tag{4.4}$$

The sun height in Figure 4.1 is the complementary angle of the zenith angle. Due to this reason it can simply be stated as:

$$\beta_s = 90 - \theta_z \tag{4.5}$$

Tracking systems for the collector are important in terms of harvesting the maximum amount of energy out of the sunlight. The standard tracking system for a parabolic trough collector is a

single axis tracking system. The collector orientation is normally either in a north-south or east-west direction. For a fixed east-west direction the surface azimuth is defined as:

$$\alpha = \begin{cases} 0 \; if \; |\alpha_s| < 90 \\ 180 \; if \; |\alpha_s| \geq 90 \end{cases} \tag{4.6}$$

Therefore the tilt angle of the surface can be calculated from:

$$\tan\beta = \tan\theta_z |\cos\alpha_s| \tag{4.7}$$

The aim of the one axis tracking system is to minimize the angle of incidence. For tracking in north south direction the angle can be evaluated according to:

$$\cos\theta = \sqrt{(1 - cos^2\delta sin^2\omega)} \tag{4.8}$$

The same calculations can be undertaken for a fixed north-south orientation of the collector surface. Here the surface azimuth is defined by:

$$\alpha = \begin{cases} 90 \; if \; \alpha_s > 0 \\ -90 \; if \; \alpha_s \leq 0 \end{cases}, \text{ This depends on the sign of the solar azimuth angle} \tag{4.9}$$

Consequently, the collector tilt angle is evaluated according to the following equation:

$$\tan\beta = \tan\theta_z |\cos(\alpha - \alpha_s)| \tag{4.10}$$

The incidence angle for a plane rotating about a horizontal north-south axis, with continuous tracking, is:

$$\cos\theta = \sqrt{(cos^2\theta_z + cos^2\delta sin^2\omega)} \tag{4.11}$$

Based on the angles described in this chapter it is possible to calculate the incoming beam radiation on a collector field, with one axis tracking system for a certain location and time. Figure 5.2 of the next chapter shows the plot of these angles versus time.

4.2 Sun Collector Geometry

For CSP operation around 400^{O}C is necessary. With a flat plate collector, this high temperature cannot be achieved. Therefore concentrating collector such as parabolic trough collector is used. The direct normal radiation reaching the collector is concentrated on the absorber tube located at the focal point of the parabolic collector. The most important characteristic factor therefore, is the concentration ratio. It is defined as the aperture area in relation to the absorber area and for parabolic trough a maximum concentration ratio of 200 can be reached.

The most significant losses under some circumstances occurring in a solar field are the shading losses. This reduction is happening when one collector row reflects its shadow onto the next row. In well-designed CSP plants this effect only shows up in the morning or evening hours with shadowing due to low tilt angle. However at these times shading losses can reach a maximum of up to 100%, where the rest of the day these losses are close to zero. The part of the collector area that is not in the shaded region, can be approximately calculated according to Stuetzle, 2002 as:

$$\xi_{SL} = \frac{D}{W}\frac{cos\theta_z}{\cos\theta} \tag{4.12}$$

where ξ_{SL} is 0, which means complete shading, and 1, which means no shading of collector.

$$\xi_{SL} = \min\left[\max\left(0; \frac{D}{W}\frac{cos\theta_z}{\cos\theta}\right); 1\right] \tag{4.13}$$

It is obvious that the shading effect is dependent on the collector size and the distance between the collector rows. In the above equation,

D is the distance between collector rows in meters; and

W is the collector aperture width in meters

Another loss factor occurs because, the incoming radiation to the collector is not exactly perpendicular and the absorber tube has a finite length. At the end of each collector a certain part of the absorber tube will be not be irradiated. Normally these losses are under 2% sin feasible areas for CSP plants. Nevertheless, the reduction factor can be calculated according to:

$$l = f tan\theta \tag{4.14}$$

Where, l is length of the not irradiated part, which depends on the collector design, while f is the focal length. Consequently, the losses in percentage according to Lippke, 1995 where L is length of collector can be calculated as:

$$\xi_{EV} = 1 - \frac{l}{L} \tag{4.15}$$

Further losses that occur depend on the finite earth sun distance where the beams reaching the collectors are also not exactly parallel. As a result the sun image on the absorbers is not precisely circular. The image can be seen in the form of an ellipse, which changes the frame, depending on the angle of incidence. Only for θ equal to zero the image will be circular. By increasing the incidence angle the performance characteristic of the sun image becomes worse. This happens because the absorber is designed for a perfect circular sun image. This effect is called incidence angle modifier and can be predicted according to Marco (1995) as follows:

$$\xi_{IAM} = \cos\theta(1 + sin^3\theta) \tag{4.16}$$

From this formula we can observe that the losses occurring are negligible. Nevertheless, they do increase with distance from the equator.

Finally the irradiation reaching the collector can be separated in two parts. One is exactly perpendicular the other one is horizontal to the collector. The collector however only can reflect the perpendicular part of the radiation. This leads to the so called cosine-effect. Here the amount of useful irradiation can be calculated by:

$$\xi_{COS} = \cos\theta \tag{4.17}$$

Chapter 5: Simulation Framework of Model

5.1 Program Overview

The simulation is intended to accurately reproduce of the thermodynamics process occurring in parabolic trough concentrated solar power plant located in the North-eastern part of Ethiopia. At the moment, not even one CSP plant, exclusively powered by solar energy is installed in Ethiopia. Consequently, predictions for the future have to be undertaken. To make these predictions reasonable, information about potential and available areas is taken and processed in realistic way for a further performance calculation. The following flow chart gives common overview of how this is put to execution.

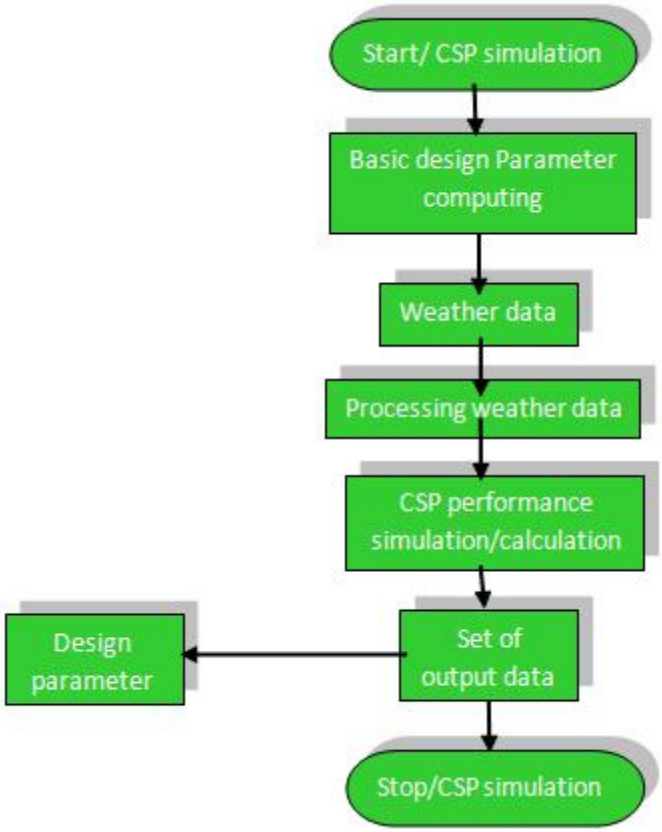

Figure 5.1: Basic program structure for computing CSP power output

The first program step evaluates all the necessary angles for predicting the sun position at a specific location and time. The necessary geometrical calculations are explained in the previous chapter Solar Geometry where one axis tracking system is assumed for the solar field.

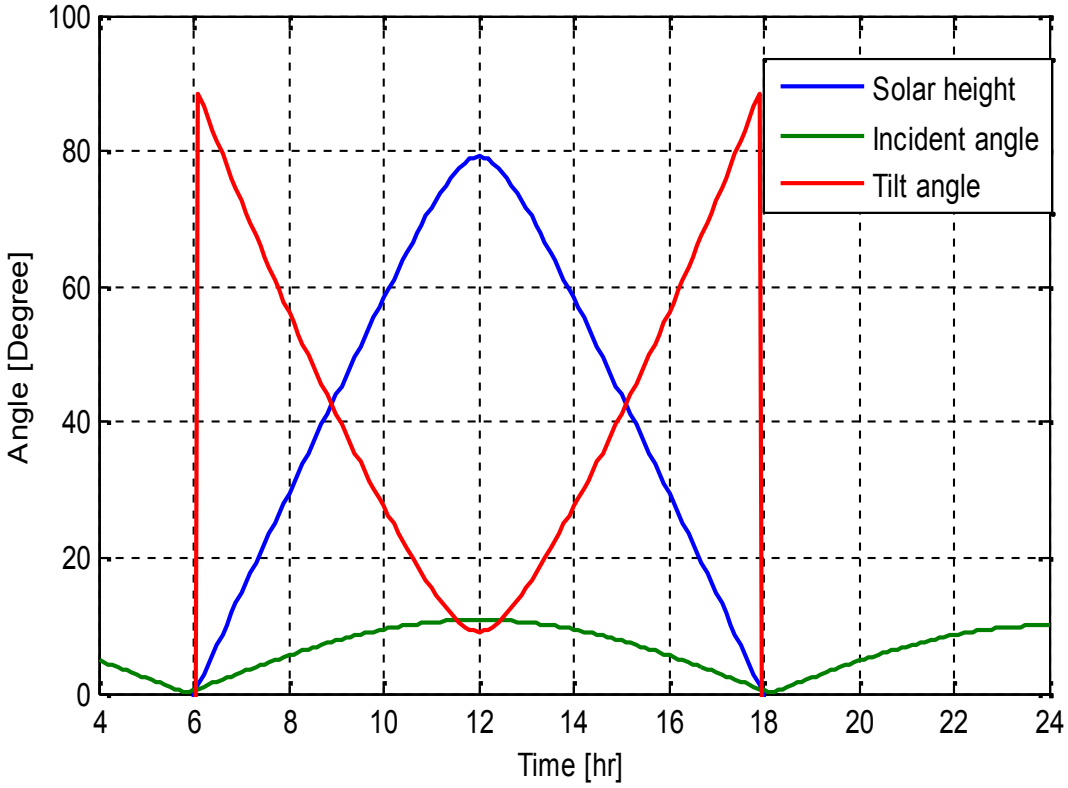

Figure 5.2: Incident angle, tilt angle, and solar height at latitude 10.41^{O} and longitude 42.21^{O} for March 21

It can be noticed that the tracking system first starts with sunrise and stops with sunset. The maximum allowed angle for the system is 90° in east west direction. To proceed further, the design parameters for the solar field must be defined. These parameters are essential for predicting the thermal energy output of the solar field. The design parameters have to be set manually before starting the simulation. Values for the common LS-2 system are shown in Table 5.1.

Table 5.1: Design parameter for simulation of solar field for plant with capacity of 30 MW

Parameter	Value	Type
Distance between collector row [m]	15	LS-2
Height of the collector [m]	5	LS-2
Length of the collector [m]	49	LS-2
Focal length of the collector [m]	5	LS-2
Inlet temperature of the heat transport medium [^{O}C]	297.8	LS-2
Outlet temperature of the heat transport medium [^{O}C]	390.5	LS-2
Solar field coefficient [%]	0.99	LS-2
Transmission coefficient of the piping [%]	0.95	LS-2
Areas of the collector field [m^2]	182,000	30 MW Capacity
Availability of the solar field [%]	0.995	

The part geometrical losses focus on the calculation of losses depending on incident angle, shading losses and the axial end losses.

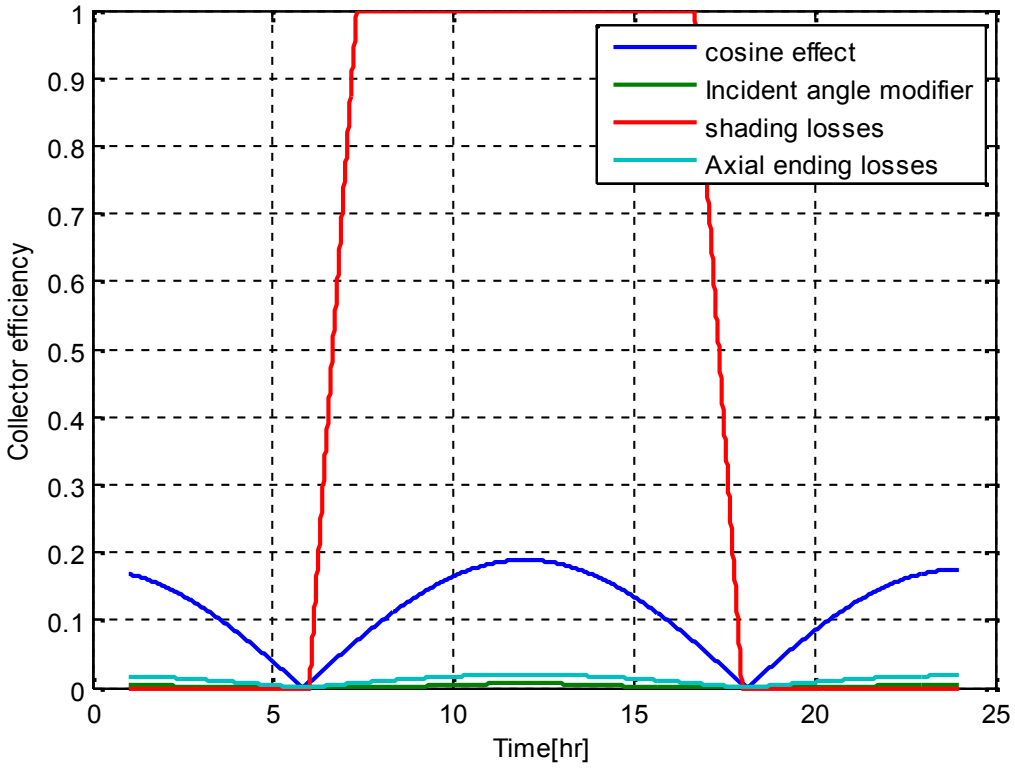

Figure 5.3: Geometrical collector losses at latitude 10.41^{O} and longitude 42.21^{O} for March 21 for one axis tracking system, collector orientation north south.

Figure 5.3 shows that the axial ending losses as well as shading losses having nearly no effect during the daily operation. Shading losses only occur in the morning and evening hours. The losses of the incidence angle modifier can be seen as constant during the day, but these losses are always under 5%, in the areas of interest. Therefore the only significant geometrical losses are represented by the cosine losses.

Now all necessary relations for the description of how the energy provided by the sun is harvested and distributed to the power block are described. The point of interest is now power block arrangements.

5.2 Flow Diagram for Power Cycle -State Points

A model of 30 MW CSP system is constructed using data from an existing 30 MW SEGS VI plant. The power cycle begins by collecting the HTF returning from the solar field in an

expansion vessel. The expansion vessel serves to compensate for variation in the volume of the heat transfer fluid throughout the day, since the specific volume of the HTF is dependent on temperature. The heat transfer fluid is pumped from the expansion vessel and delivered to two parallel heat exchanger trains as the energy source for the power cycle. The first heat exchanger train consists of a superheater, steam generator, and preheater, in series, and the second consists a reheater.

The HTF receives pre-heated feedwater and generates dry steam by heat exchange with the HTF in the steam preheater, steam generator, and superheater. The superheated steam travels first through the high pressure turbine, where it expands and propels the turbine blades. Two extractions are taken from the high pressure turbine; these extracted steam lines are used to preheat feedwater in two closed feedwater heaters FWH 4 and FWH 5. Upon exiting the high pressure turbine, the steam is directed through a reheater, where it is superheated to approximately the same temperature reached at the outlet of the superheater. The superheated steam then passes through the low pressure turbine, where again the steam expands and propels the turbine blades. Four steam extractions are taken from the low pressure turbine; one is directed to the deaerator, and the remaining three are fed to feedwater heaters 1 – 3. The steam leaving the low pressure turbine is condensed in a surface condenser by heat exchange with circulating water. The condensed steam (now referred to as feedwater) is pumped to a sufficiently high pressure to allow it to pass through the three low pressure feedwater heaters and into the deaerator. The feedwater is pumped again at the outlet of the deaerator, to a pressure slightly higher than the boiling pressure in the steam generator. Feedwater passes through the two high pressure feedwater heaters before returning to the preheater to complete the cycle.

The temperature, pressure and enthalpy at each state point in the system for gross power of 35 [MWe] with 100% solar operation are provided in the technical feasibility assessment of the plant [13]. This state is referred to as the ‘reference’ state for the power plant.

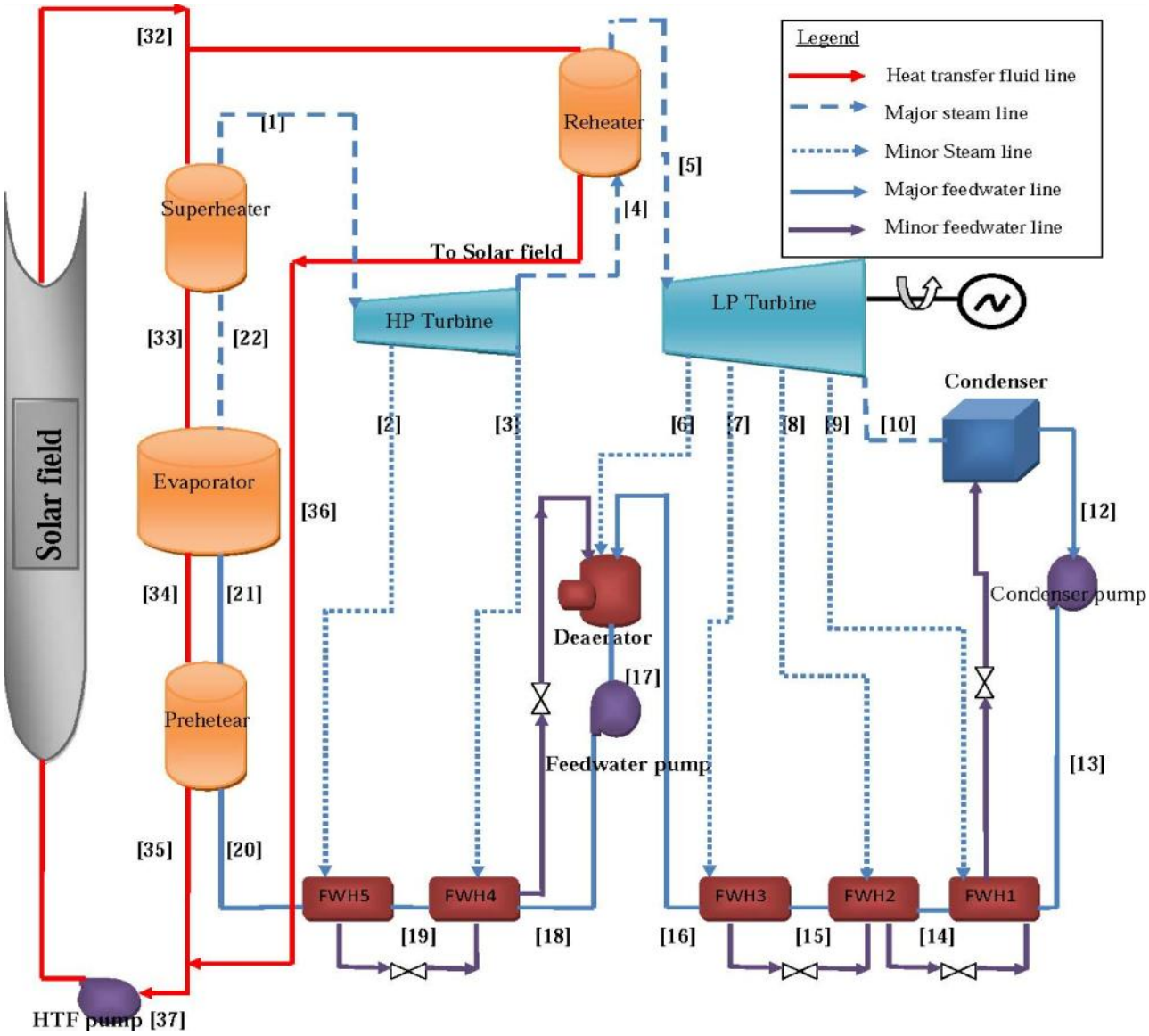

Figure 5.4: Flow diagram for power cycle - state points

5.3 TRNSYS Model of SEG VI Power Plant Using STEC Library

In this work a mode of a solar thermal electric generating system using parabolic trough collector is created using components from the STEC library. Detailed information about these components is given below. A schematic of the model is shown in the TRNSYS simulation studio in Figure 5.5.

The boiler section of the system consists of the superheater, the steam generator and the preheater. The links between the components consider two fluid circuits: the heat transfer fluid (HTF), which flows from the HTF splitter in the solar field model, and the water steam circuit which flows from the high pressure closed feed water heater.

The boiler is then linked to a steam turbine with five extraction lines is presented by with two high pressure and five low pressure turbine stages and four extraction splitters. Between the high and low pressure turbine stages a reheater (Reheater) exists. The final turbine stage is connected to the condenser component (Condenser).
The extraction splitters are connected to the two high and three low pressure closed feed water heaters (FWH1, FWH2, FWH3, FWH4, FWH5) and a deaerator. The relevant links between the TRNSYS components in the modeling of the power plant are discussed as it follows:

- The evaporator cold side flow rare demand is linked to desired mass flow rate of the feedwater pump as an input which sets the flow rate of the whole system.
- Flow rate and enthalpy are connected from turbine stage outlet to splitter and further from the splitter outlet to the turbine stage inlet. The pressure is connected in the opposite direction from condenser to turbine stage outlet to splitter inlet and so on. Pressure and enthalpy are connected from the splitters outlet to the closed feed water heaters and deaerator inlet whereas the steam flow rate (demand) is connected in the opposite direction.
- The feedwater flow rate and temperature from the condenser outlet is linked first to the pump, then to the five low pressure closed feed water heater, then to the deaerator, then to the feedwater pump, then to the two high pressure closed feed water heater and then to the preheater inlet.
- The quality and flow rate of the condensed extraction steam in the closed feed water heater is linked to the condensate inlet of the closed feed water heaters and deaerator.

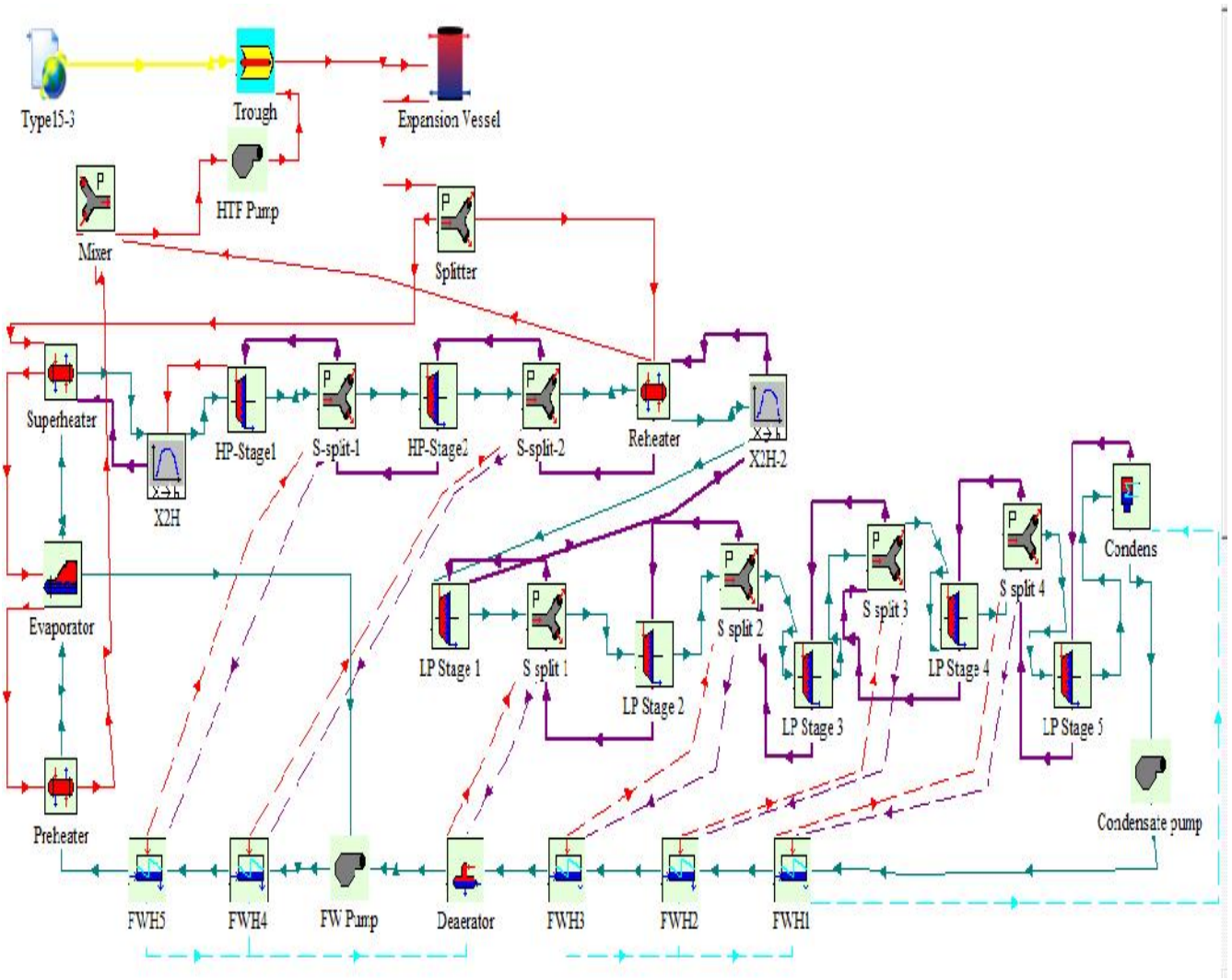

Figure 5.5: The SEGS VI TRNSYS Model using STEC library

5.3.1 Superheater

The superheater model used in this system is a tube and shell heat exchanger from STEC built-in component Type 315. Values for constant parameters and initial conditions used are taken from a technical description by Lippke, 1995. The effectiveness of the superheater is related to its thermal performance. The heat exchanger effectiveness (ε) is defined as the actual heat transfer realized between streams ($\dot{Q}_{max}$) over the maximum heat transfer possible for the given streams (max) [13]. Figure 5.6 shows the flow diagram for the superheater.

$$\varepsilon = \frac{\dot{Q}}{\dot{Q}_{max}} \tag{5.1}$$

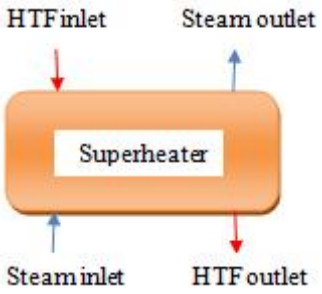

Figure 5.6: Flow diagram of superheater

Table 5.2: Constant parameters and initial conditions for superheater

Parameter	Input
Overall heat transfer coefficient [kJ/hr K]	1015.97
Hot side inlet temperature [°C]	390.56
Hot side flow rate [kg/s]	396.4
Cold side inlet temperature [°C]	297.8
Cold side flow rate [kg/s]	38.969
Cold side quality [-]	1
Cold side outlet pressure [bar]	100
Hot side specific heat [kJ/hrK]	2.59

For all heat exchangers, the hot side is the HTF flowing from the collector while the cold side is the water in the Rankine cycle. The transient values for inputs for the superheater are defined by the input connections given in Table 5.3, while the outputs that define transient inputs for other components are given in Table 5.4.

Table 5.3: Input links for the superheater

Input	Output
Superheater	Splitter
Hot side flow rate	Outlet flow rate2
Superheater	Boiler
Cold side inlet temperature	Cold side outlet temperature
Cold side flow rate	Cold side outlet flow rate
Cold side quality	Cold side quality
Superheater	X2H
Cold side outlet pressure	Steam pressure

X2H is a STEC component which converts steam properties given by T, p, and x used in the superheater and reheater components to h and p used in the turbine stage components.

Table 5.4: Output links for the superheater

Input	Output
Boiler	Superheater
Hot side inlet temperature	Hot side outlet temperature
Hot side flowrate	Hot side flowrate
Cold side outlet pressure	Cold side inlet pressure
X2H	Superheater
Steam temperature	Cold side outlet temperature
Steam quality	Cold side outlet quality
Steam flow rate	Cold side flow rate

5.3.2 Evaporator/Boiler

The feed water enters the shell side of the boiler and exits as a saturated vapor. STEC built-in component Type 316 is used to model a boiler. The boiler effectiveness is related to the number of transfer units (NTU). In changing phase from saturated liquid to saturated vapor, the heat capacitance of the feedwater/steam is infinite. Therefore, the minimum capacitance of the two fluids will always be the capacitance of the hot side fluid (the heat transfer fluid) [13]. Figure 5.7 shows the flow diagram for the boiler. The minimum capacitance of the fluid is:

$$C_{MIN} = \dot{m}_{HTF}\left(\frac{h_{HTF,in} - h_{HTF,out}}{T_{HTF,in} - T_{HTF,out}}\right) \tag{5.2}$$

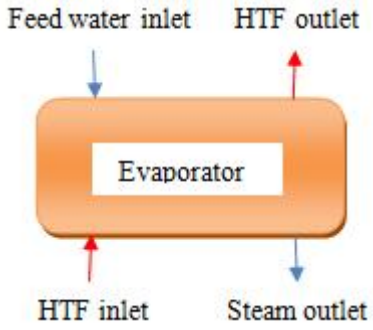

Figure 5.7: Flow diagram of evaporator/boiler

5.3.3 Preheater

The preheater is also a type of heat exchanger and is used to raise the temperature of the feed water leaving the system of feed water heaters. STEC built-in component Type 315 is used to model a preheater. While modeling the preheater, it is assumed that the feedwater outlet state will be saturated liquid at the outlet pressure of the preheater [13]. The heat transfer to the feedwater is calculated from:

$$\dot{Q} = \dot{m}_{feedwaer}\left(h_{feedwater,out} - h_{feedwater,in}\right) \tag{5.3}$$

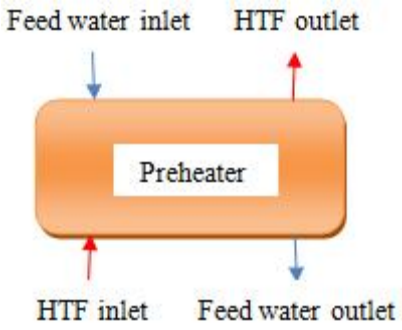

Figure 5.8: Flow diagram of preheater

5.3.4 Turbine (High Pressure and Low Pressure)

Superheated steam leaves superheater at high temperature and pressure and enters high pressure (HP) turbine. The expansion of the steam as it moves from higher to lower pressure (LP) converts the steam's enthalpy to shaft work. During the expansion processes steam is extracted and fed to the feed water heaters. The turbines are modeled as connection of series turbine stages. Each stage consists of one turbine along with one splitter. One outlet of the splitter is connected to the next turbine and the other to a feed water heater.

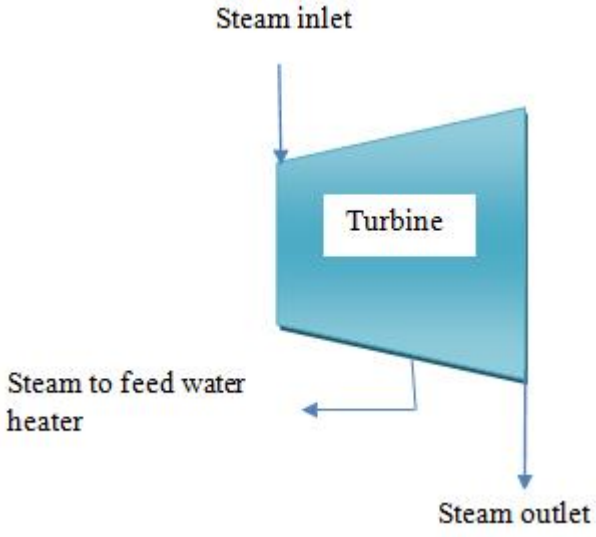

Figure 5.9: Flow diagram of turbine stage with turbine and splitter

The high pressure (HP) turbine consists of two stages and the low pressure (LP) turbine consists of five stages. Between the HP and LP turbines steam passes through the reheater to increase the cycle efficiency. The thermodynamic performance of each turbine stage is described by its

isentropic efficiency [13]. The isentropic efficiency of a turbine stage is equal to the change in enthalpy of the fluid to the change in enthalpy of an isentropic (adiabatic and reversible) turbine:

$$\eta = \frac{h_{steam,in} - h_{steam,out}}{h_{steam,in} - h_{steam,out,s}} \tag{5.4}$$

where-: $h_{steam,out,s}$ is the enthalpy that would have occurred at the outlet of the isentropic turbine.

The total power of the turbine is equal to the mass flow rate through each turbine stage multiplied by the specific work of that stage. The steam mass flow rate through each stage is equal to turbine inlet mass flow rate minus the total mass flow rates of the steam extracted to flow to the feedwater heaters in the previous stages. The power for each turbine stage is described as follows:

$$\dot{W}_{HP1} = \dot{m}_1 \dot{w}_{1-2} \tag{5.5}$$

$$\dot{W}_{HP2} = (\dot{m}_1 - \dot{m}_2) \dot{w}_{2-3} \tag{5.6}$$

$$\dot{W}_{LP1} = \dot{m}_5 \dot{w}_{5-6} \tag{5.7}$$

$$\dot{W}_{LP2} = (\dot{m}_5 - \dot{m}_6) \dot{w}_{6-7} \tag{5.8}$$

$$\dot{W}_{LP3} = (\dot{m}_5 - \dot{m}_6 - \dot{m}_7) \dot{w}_{7-8} \tag{5.9}$$

$$\dot{W}_{LP4} = (\dot{m}_5 - \dot{m}_6 - \dot{m}_7 - \dot{m}_8) \dot{w}_{8-9} \tag{5.10}$$

$$\dot{W}_{LP5} = (\dot{m}_5 - \dot{m}_6 - \dot{m}_7 - \dot{m}_8 - \dot{m}_9) \dot{w}_{9-10} \tag{5.11}$$

The total output equals the sum of the output from each turbine section.

$$\dot{W}_{Turbine} = \dot{W}_{HP1} + \dot{W}_{HP2} + \dot{W}_{LP1} + \dot{W}_{LP2} + \dot{W}_{LP3} + \dot{W}_{LP4} + \dot{W}_{LP5} \tag{5.12}$$

In the model reference conditions for turbine section are used as shown in the Table 5.5.

Table 5.5: Reference efficiency and inlet conditions for turbine sections (Source: Kearney and Miller, 1987)

Turbine Section	Inlet pressure [bar]	Inlet enthalpy [kJ/kg]	Efficiency [-]
HP-1	100	3005	0.838
HP-2	33.61	2807	0.843
LP-1	17.10	3190	0.859
LP-2	7.98	3016	0.919
LP-3	2.73	2798	0.936
LP-4	0.96	2624	0.88
LP-5	0.29	2325	0.6445

For the HP and LP turbines, STEC components Type 318 (turbine) and Type 389 (splitter) are used to model a single turbine stage. The LP turbine stages are modeled in a manner parallel to the HP turbine stages The TRNSYS model of the high pressure turbine and low pressure turbine are represented in Figure 5.10a and Figure5.10b, respectively.

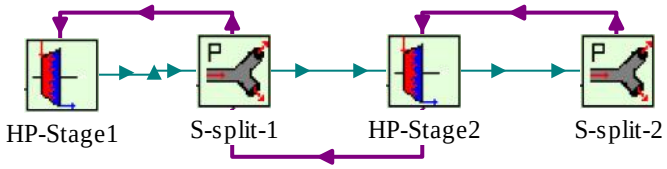

Figure 5.10a: STEC components turbine and splitters for HP turbine stage

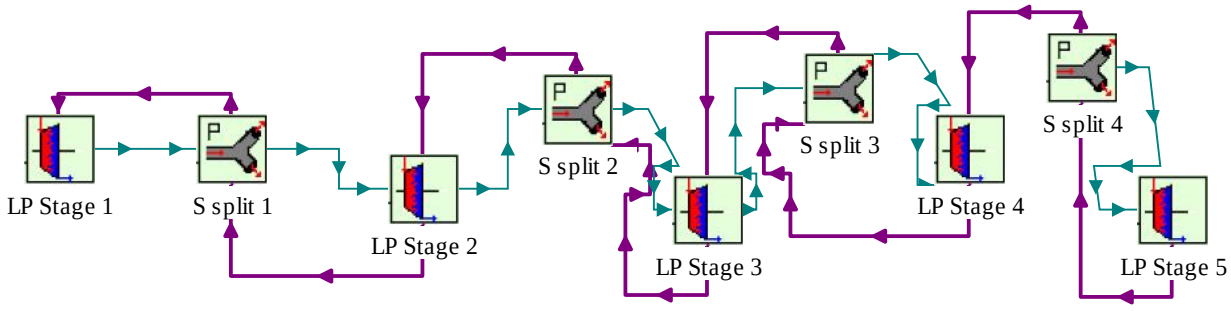

Figure 5.10b: STEC components turbine and splitters for LP turbine stage

Between the HP and LP turbines steam passes through the reheater to increase the cycle efficiency.

5.3.5 Reheater

The reheater is also a shell and tube heat exchanger. In this cycle after leaving the HP turbine the steam goes to the reheater and the temperature increases so that the system efficiency increases. The reheater model is the same as the superheater model. STEC built-in component Type 315 is used to model the reheater. Values for constant parameters and initial conditions used are given in Table 5.6.

Table 5.6: Constant parameters and initial conditions for the reheater

Parameter	Input
Overall heat transfer coefficient [kJ/hr K]	1724.11
Hot side inlet temperature [^{O}C]	390.56
Hot side flow rate [kg/s]	47.87
Cold side inlet temperature [^{O}C]	208.67
Cold side flow rate [kg/s]	33.16
Cold side quality [-]	1
Cold side outlet pressure [bar]	17.10
Hot side specific heat	2.59

5.3.6 Condenser

The condenser is a shell and tube heat exchanger. The condenser condenses the steam from the LP turbine (steam inlet) to a liquid so that the fluid can be easily pumped back to the boiler (condensed feed water outlet).

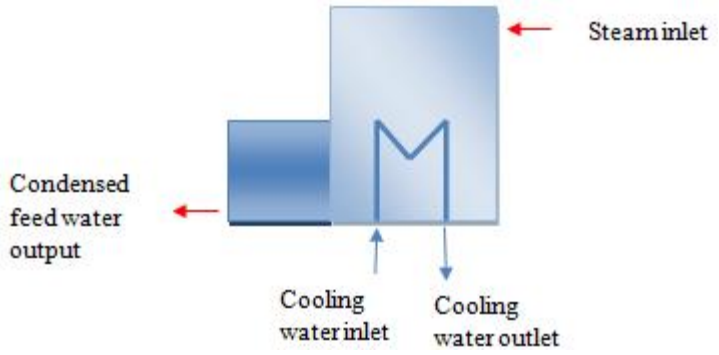

Figure 5.11: Flow Diagram of Condenser

$$\epsilon_{Condenser} \frac{\dot{Q}_{Condenser}}{\dot{Q}_{Condenser,max}} \tag{5.13}$$

The condenser effectiveness is the ratio of the heat transfer between cooling water and condensing steam to the maximum heat transfer between these streams [13].

$$\dot{Q}_{Condenser} = \dot{m}_{steam}\left(h_{steam,in} - h_{steam,out}\right) \tag{5.14}$$

$$\dot{Q}_{Condenser,max} = \dot{m}_{Condenser} \cdot \dot{c}_{Condenser}(T_{steam} - T_{condenser,in}) \tag{5.15}$$

5.3.7 Pump

Three pumping processes exist in the modeled system. The first one is heat transfer fluid pump which is located before the collector field. The second one is feedwater pump and is located at the deaerator outlet. The third one is condensate pump which is located at the condenser outlet. To model the pump STEC component Type 300 is used. Pump performance is characterized by its isentropic efficiency [13].The isentropic efficiency of the pump is:

$$\eta_{pump} = \frac{h_{feedwater,in} - h_{feedwater,out,S}}{h_{feedwater,in} - h_{feedwater,out}} \tag{5.16}$$

where: $h_{feedwater,out,S}$ is the enthalpy that would have occurred were the pumping process isentropic.

The work performed by the pump per unit mass is given by:

$$\dot{W}_{pump} = h_{feedwater,in} - h_{feedwater,out} \tag{5.17}$$

Figure 5.12: Flow diagram of a pump

5.3.8 Deaerator

Deaerator preheats the feed water for the steam generator. Steam extracted from the 1st stage of the LP turbine is directly mixed with feed water. At the outlet of the deaerator there is a feed pump which increases the fluid pressure to boiling pressure. The deaerator is a mixing device with three inlets and single outlet stream [13]. STEC component Type 384 is used to model the deaerator. The three inlets are the drain water from the high pressure feedwater heaters, the extracted steam from the first stage of the low pressure turbine, and the feedwater from the low pressure feed water heaters. The total mass flow rate is the sum of the three inlets.

$$\dot{m}_{steam,extracted} + \dot{m}_{steam,drain} + \dot{m}_{feedwater,in} = \dot{m}_{feedwater,out} \tag{5.18}$$

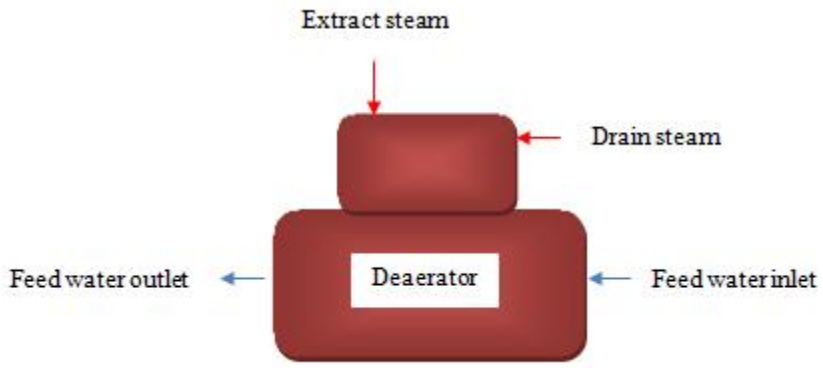

Figure 5.13: Flow diagram of a deaerator

5.3.9 Feedwater Heater

A feedwater heater increases the steam temperature and thereby reduces the heat addition from the collector loop and increases the system efficiency. For feed water heater STEC component Type 317 is used to model a feed water heater.

The size and conductance determine the feedwater heater's overall heat transfer factor (UA). An overall UA for each feedwater heater is defined assuming steam is condensing throughout the length of the feedwater heater [13].

The preheater model calculates the required steam mass flow rate that keeps the water level in this heat exchanger constant. Effective heat transfer factor describes the heat transfer characteristic. UA is evaluated as a function of the cold side flow rate from:

$$\frac{UA}{UA_{REF}} = \left(\frac{\dot{m}_{feedwater}}{\dot{m}_{feedwater,REF}}\right)^{0.8} \tag{5.19}$$

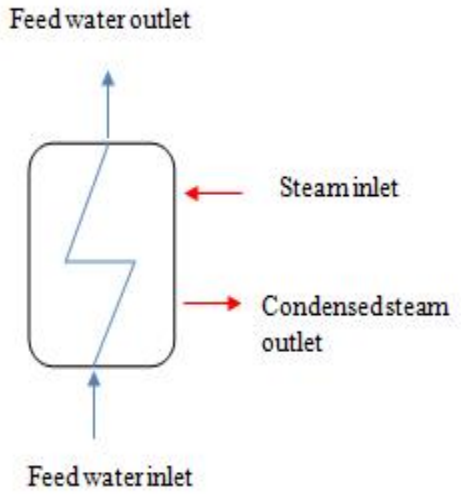

Figure 5.14: Flow diagram of a feedwater heater

5.3.10 Weather Data

This component reads weather data from a data file. Type 15 is used for reading data in EPW format. An EPW is a data file which provides standard hourly values of solar radiation and meteorological elements for a period of a year. The initial parameters that are used to model the weather data are stated below.

Table 5.7: Initial parameters for weather data

Parameter	Input
Ground reflectance [-]	0.2
Slope of surface [^{O}]	0
Azimuth of surface [^{O}]	0

5.3.11 Expansion Vessel

Expansion vessel absorbs the volume changes that take place within the heat transfer fluid circulatory system. Type 4-aof TRNSYS library is used to model expansion vessel.

Figure 5.15: Flow diagram of expansion vessel

5.3.12 Parabolic Trough

The parabolic trough collector component is developed using Lippke's model [10]. To account for changing fluid temperature, an integrated efficiency equation is used.

$$\eta = K[A + B(\Delta T)] + C\frac{\Delta T}{I} + D\frac{\Delta T^2}{I} \quad (5.20)$$

In this equation:

A: Optical efficiency of the trough and the absorptivity of the selective coating without considering the losses at the end of a collector row;

B, C and D: Describe the heat losses of the heat collecting element (HCE) as a function of operating conditions;

ΔT: Temperature difference between the HTF and the ambient [K];

K: Incident angle modifier;

I: Direct Normal Insolation [W/m^2]

The thermal performance loss coefficient A, B, C and D for the model is taken considering black chrome and vacuum tube.

STEC component Type 396 is used to model parabolic trough collector model.

5.4 TRNSYS Model for 10 MW Power Plant Using STEC Library

To minimize cost of parabolic trough power generation in a country like Ethiopia, reduction of desired power production can be one method. Considering this, the 30 MW SEGS VI power plant TRNSYS model is customized to 10 MW as shown in Figure 5.17. Same procedure is followed as the SEGS VI plant model as to model a 10 MW power plant for selected site using TRNSYS. In the process, 2-low pressure turbine stages and 2-feedwater heaters has been reduced to get the desired output. As a consequence, Pressure optimization is done for the turbine stages using MATLAB and it is shown in Table 5.8. A MATLAB code is used to find the initial pressure after giving first guess for the initial pressure and checking the error. This pressure is found for initial steam temperature of 371 ^{O}C.

Table 5.8: Inlet and outlet conditions for turbine sections

Turbine Section	Inlet pressure [bar]	Inlet enthalpy [kJ/kg]
HP-1	100	3000
HP-2	45	2855
LP-1	16.7	3199
LP-2	4.69	2922
LP-3	0.861	2655

The state point of the 10 MW power plant is shown in Figure 5.16.

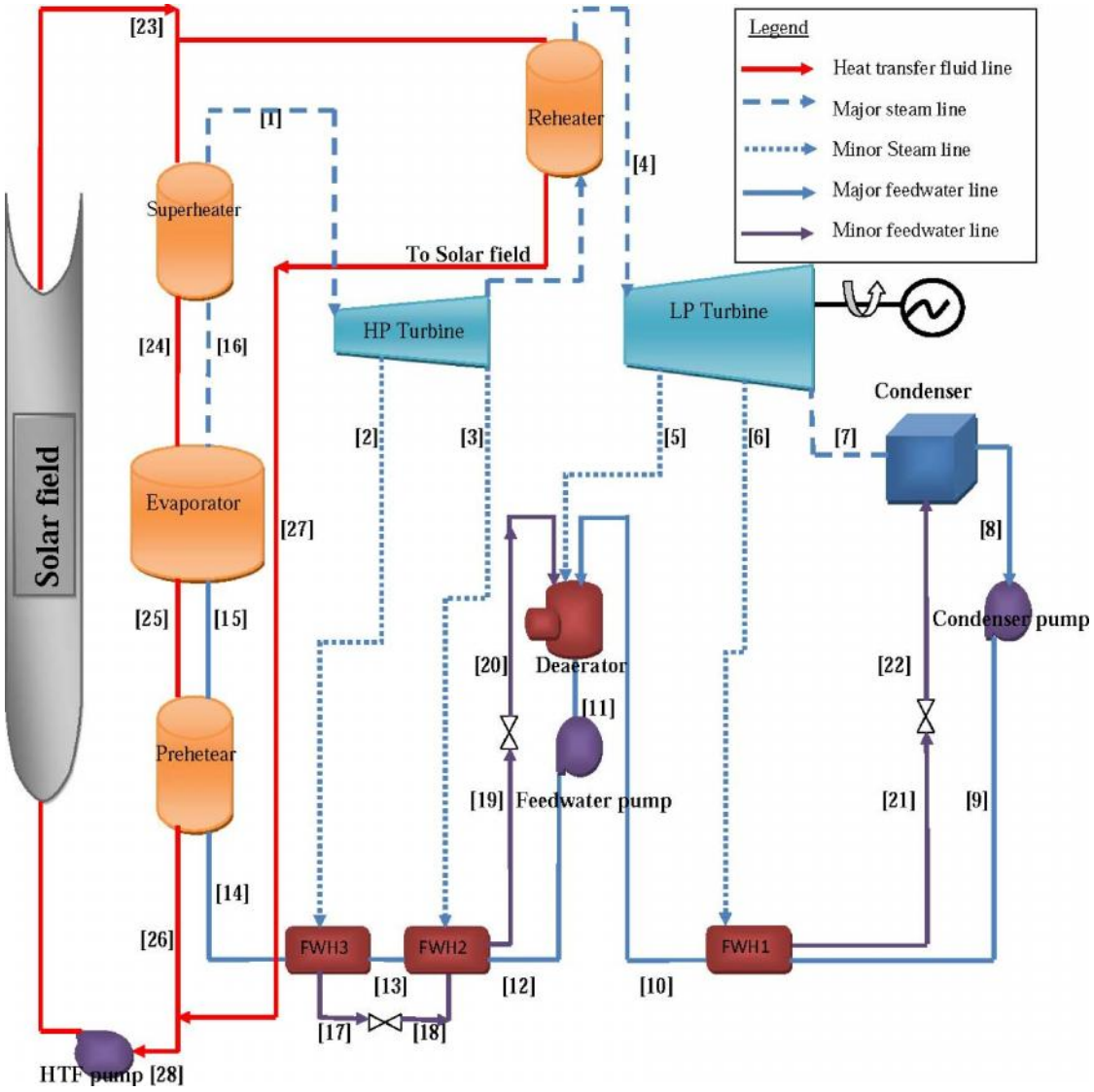

Figure 5.16: Flow diagram for power cycle - state points for 10 MW

The initial temperature of steam entering to the first high pressure turbine can be decided by assuming that the inlet temperature of the HTF in to the superheater. Therminol-VP1 stays liquid up to a temperature of 400 ^{O}C. In this designed power plant the inlet HTF temperature is taken to be 390 ^{O}C. Considering the initial temperature of steam entering to the first high pressure turbine

cannot be greater than 390 ^{O}C, the current analysis a temperature equal to T =371 ^{O}C is taken as the initial temperature of steam entering to the first high pressure turbine.

A simple approach based on physical reasoning from an efficiency point of view, has been considered to optimize the corresponding pressures. The role of feedwater heaters is to bring the temperature of the feedwater as close as possible to that of the steam generator before the feedwater enters the steam generator.

Thus the optimum, from an efficiency point of view, of the pressure at which the feedwater heaters are to be placed is obtained by finding the temperature difference that would divide the temperature difference between the boiler (saturation temperature of the boiler) and the condenser temperature into equal parts that are equivalent to the number of feedwater heaters [17].

$$\Delta T_{opt} = \frac{T_b - T_c}{n + 1} \tag{5.21}$$

where: ΔT_{opt} = Temperature rise between feedwaters

T_b = The saturated temperature of the boiler

T_c = The condenser temperature, and

n = The number of feedwater heaters

The saturation temperature for this boiler pressure is T_b = 311 ^{O}C. The condenser pressure is selected to be equal to 8 kPa. This pressure is selected taking the cooling water inlet temperature equal to atmospheric temperature (near to 25 ^{O}C). In the condenser the cooling water is designed to have a temperature rise of 10.5 ^{O}C. The terminal temperature difference is selected to be equal to 5 ^{O}C. This gives the condenser temperature T_C = 41.5 ^{O}C. The corresponding saturation pressure for this condenser temperature is equal to 8 kPa.

It has been indicated that in this analysis there are three closed feedwater heaters and one open feedwater heater. Thus the total number of feedwater heaters is four. Finally the optimum temperature difference can be calculated as shown below:

$$\Delta T_{opt} = \frac{311-41.5}{4+1} = 53.9\ ^{O}C$$

The temperature of the low pressure heater, FWH1 becomes:

$$T_{FWH1} = T_C + 53.9 = 95.4\ ^{O}C$$

The corresponding saturation pressure for this temperature is equal P (6) = 86.1 kPa.
Similar analysis is done for the remaining closed feedwater heaters and the deaerator.

State Point Temperature Determination

Name	Temperature	P_{Sat}
FWH1	$T_{FWH1} = T_C + 53.9 = 95.4\ ^{O}C$	0.861 bar
Deaerator	$T_{Deaerator} = T_{FWH1} + 53.9 = 149.3\ ^{O}C$	4.69 bar
FWH2	$T_{FWH2} = T_{Deaerator} + 53.9 = 203.2\ ^{O}C$	16.7 bar
FWH3	$T_{FWH3} = T_{FWH2} + 53.9 = 257.1\ ^{O}C$	45 bar

The overall heat transfer coefficients of the feedwater heaters and heat exchangers are also modified for the 10 MW plant TRNSYS model and are shown in Table 5.10 and Table 5.11 respectively.

.

Table 5.9: State points of the power plant (Figure 5.16)

State point	P [bar]	T [C]	h [kJ/kg]	s [KJ/kg.K]
1	100	371	3000	6.07
2	45	271	2855	6.12
3	16.7	203	2699	6.18
4	16.7	371	3199	7.12
5	4.69	229	2922	7.22
6	0.861	95.5	2655	7.35
7	0.08	41.5	2355	7.52
8	0.08	41.5	174	0.593
9	4.69	41.6	174	0.593
10	4.69	95.4	400	1.25
11	4.69	149	630	1.84
12	100	151	644	1.84
13	100	203	868	2.34
14	100	257	1122	2.85
15	100	311	1411	3.36
16	100	311	2722	5.61
17	45	257	1122	2.86
18	16.7	203	1122	2.9
19	16.7	203	868	2.36
20	4.69	149	868	2.4
21	0.861	95.5	400	1.26
22	0.08	41.5	400	1.31

Table 5.10: Overall heat transfer coefficient of the feedwater heaters

Feedwater Heaters	UA [kW/k]
FWH1	388.843
FWH2	258.959
FWH3	105.861

Table 5.11: Overall heat transfer coefficient of the heat exchangers

Feedwater Heaters	UA [kW/k]
Superheater	109.791
Steam Generator	528.811
Preheater	151.543
Reheater	101.865

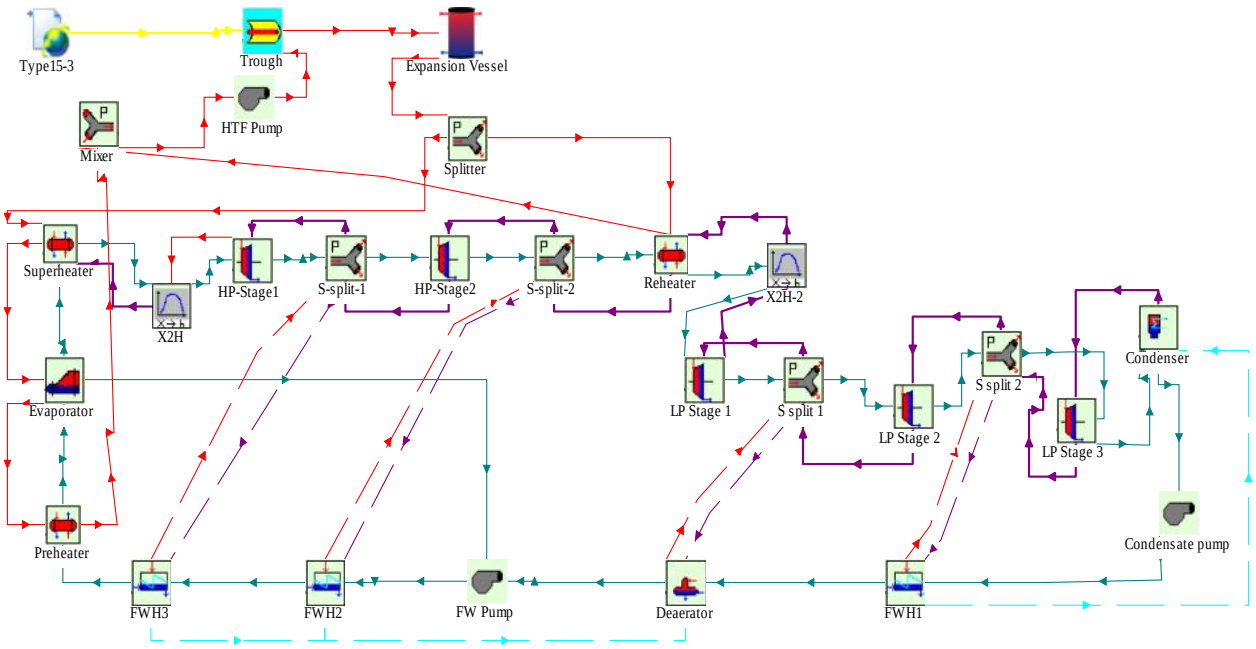

Figure 5.17: Power plant model using TRNSYS and STEC library for 10 MW

The T-S diagram for 10 MW power plant is shown in Figure 5.18.

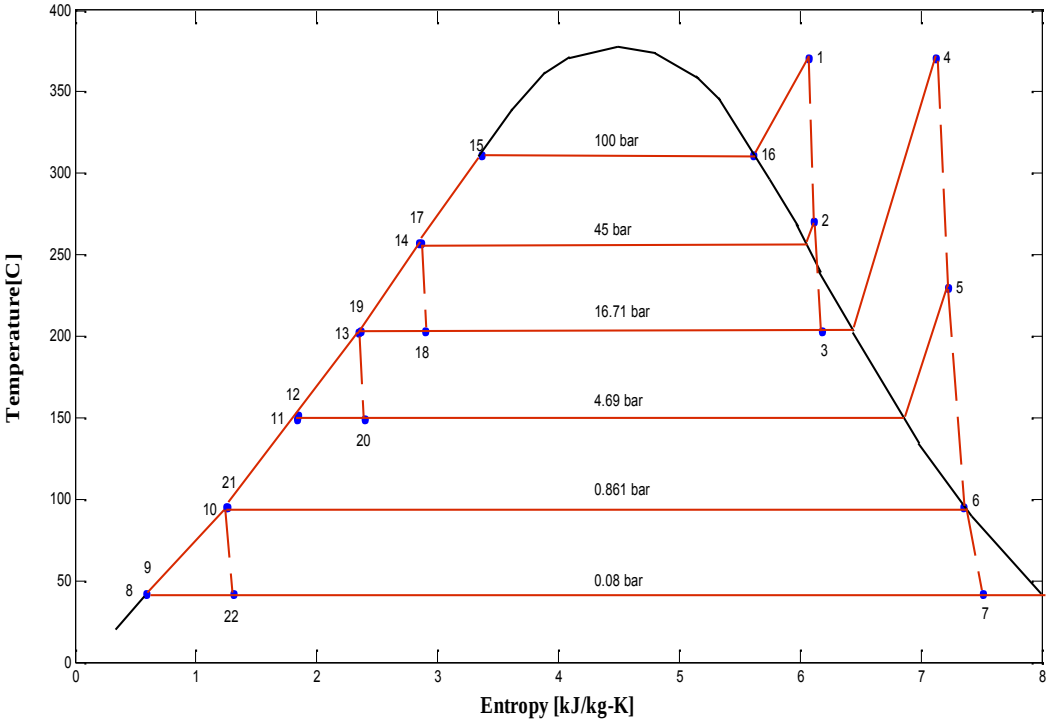

Figure 5.18: T-s diagram of 10 MW power plant

Chapter 6: Results

6.1 Model Validation

A model is created that predicts SEGS VI plant behavior and the same model is applied to Ethiopia. In order to validate the model its results are compared with measured plant data which is taken from the Kearney et al. technical description and the TRNSYS model predictions [10]. The study by Kearney et al. shows how their model's predictions compare to real operating data for a sunny summer and a cloudy winter day. Figure 6.1 shows the insolation, temperature and wind speed measured during a clear sunny day on July 18, 1991 in California, Daggett.

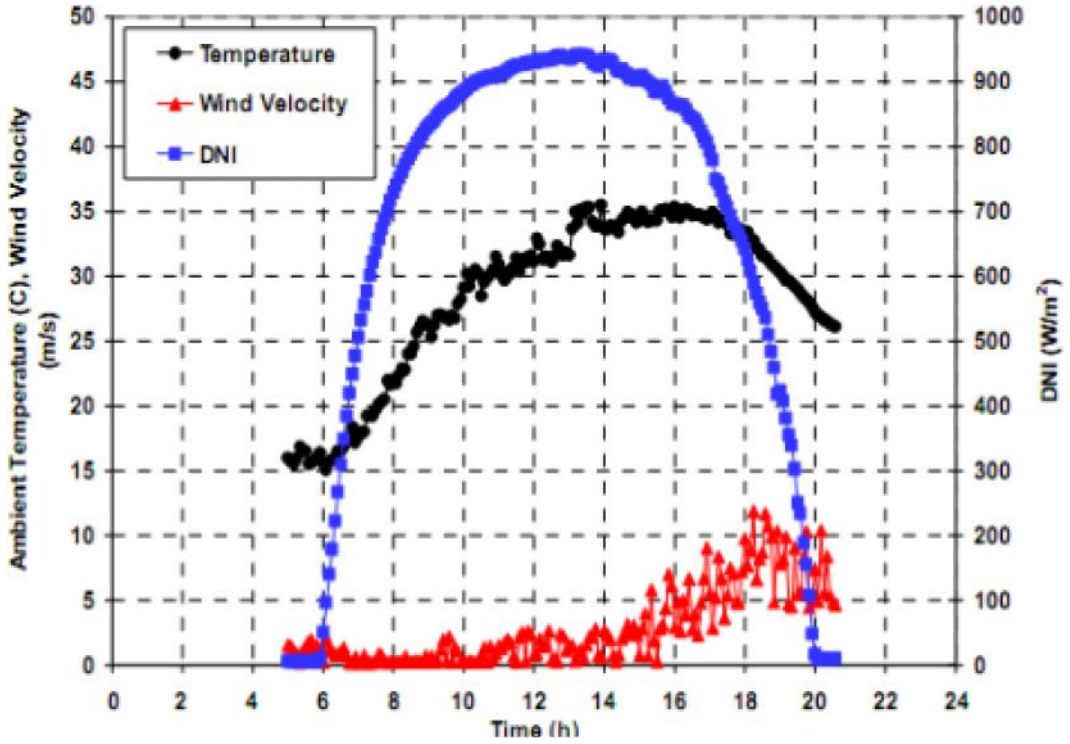

Figure 6.1: Weather conditions of July 18, 1991 [16]

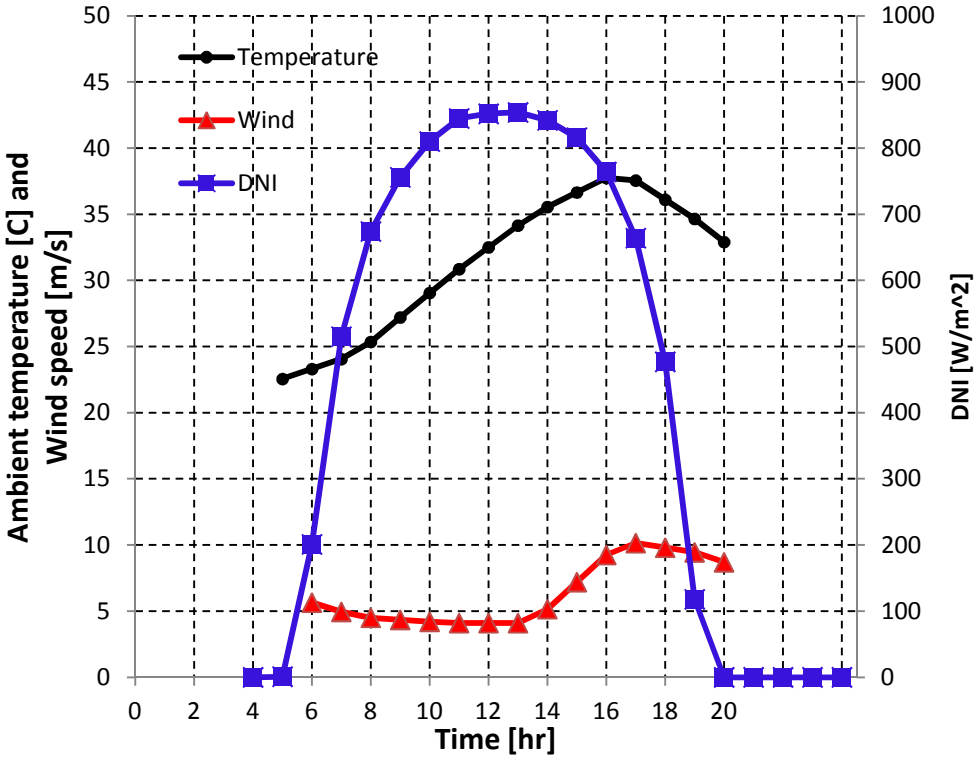

Figure 6.2: Weather conditions July 18, 1991 TRNSYS results

Figures 6.2 represents results run by TRNSYS of modeled power plant with the same data as Figure 6.1.The comparison is in close agreement and the difference is in the range of 60 $W/m^2$and 3 ^{O}C of temperature on hourly basis.

For the same above reasons there is a deviation at the beginning and end of the day. In other words, deviations occur only at the start-up and shut-down processes.

Figure 6.3 shows measured and predicted gross power output results on July 18, 1991 as reported in [16] and in Figure 6.4 the predictions from the current model are presented. As seen in the present TRNSYS simulation results are compared to that presented in the literature, the sunny day power predictions match well.

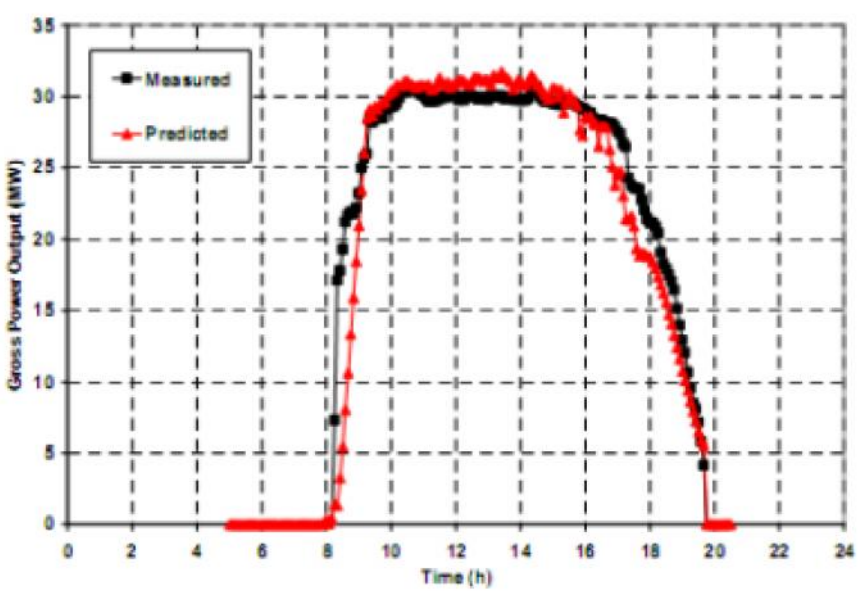

Figure 6.3: Measured and predicted gross power output on July 18, 1991 [16]

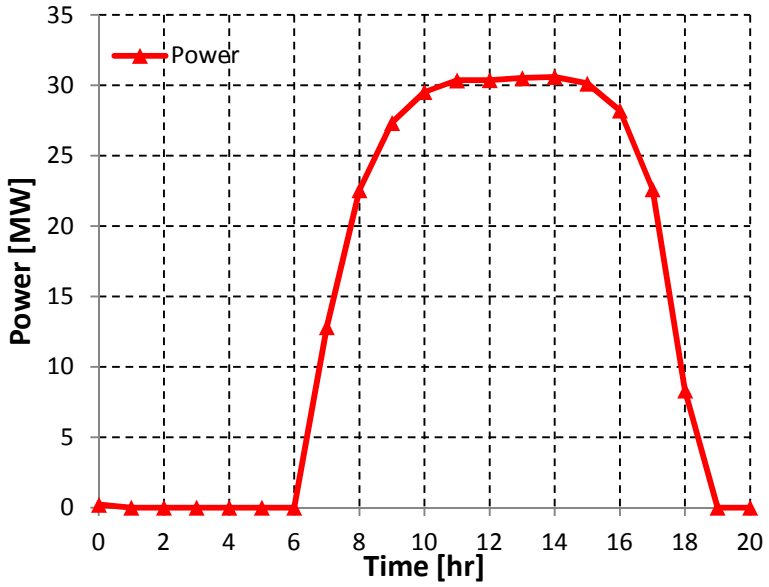

Figure 6.4: Gross power output TRNSYS result for July 18, 1991

6.2 Simulation of the selected site

The annual TRNSYS output of direct normal radiation (DNI) of Adigala is represented in Figure 6.5.The maximum DNI occurs in January.

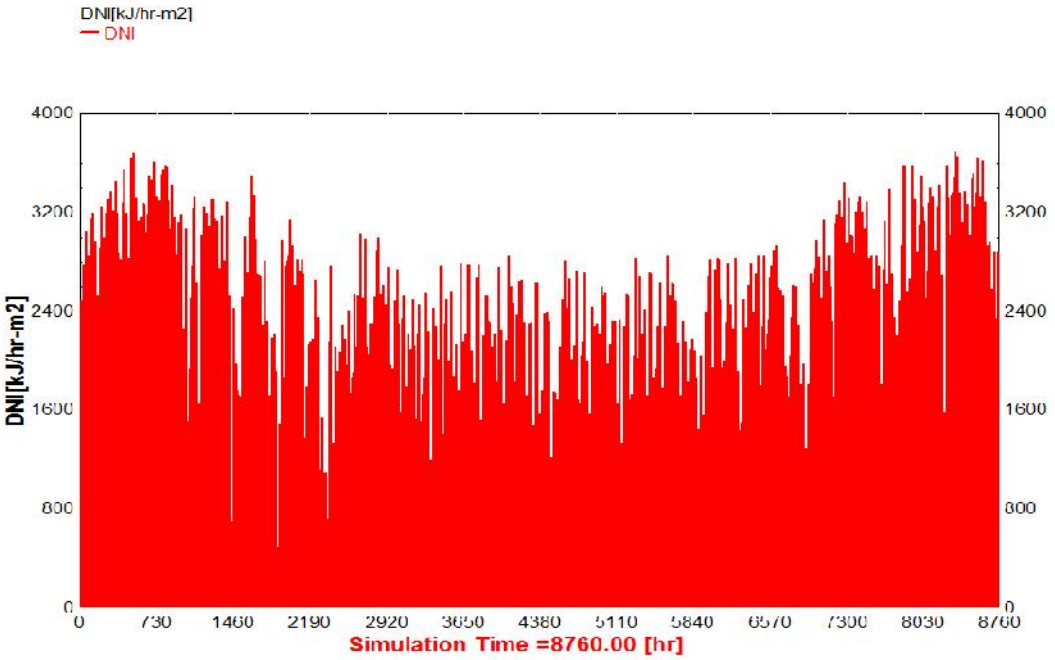

Figure 6.5: Annual output of direct normal radiation

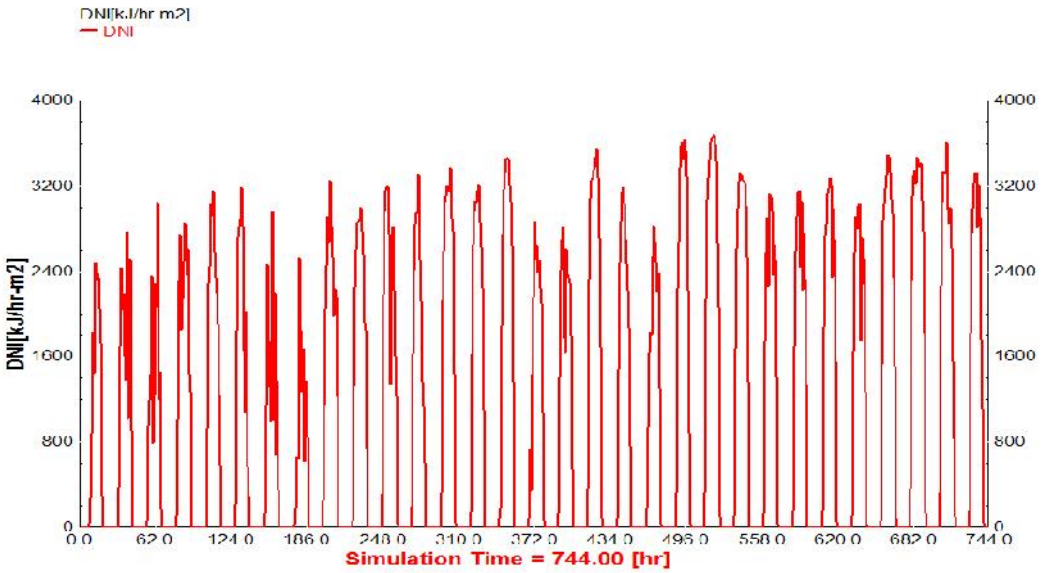

Figure 6.6: Daily output of direct normal radiation from January1 to 31, 2001

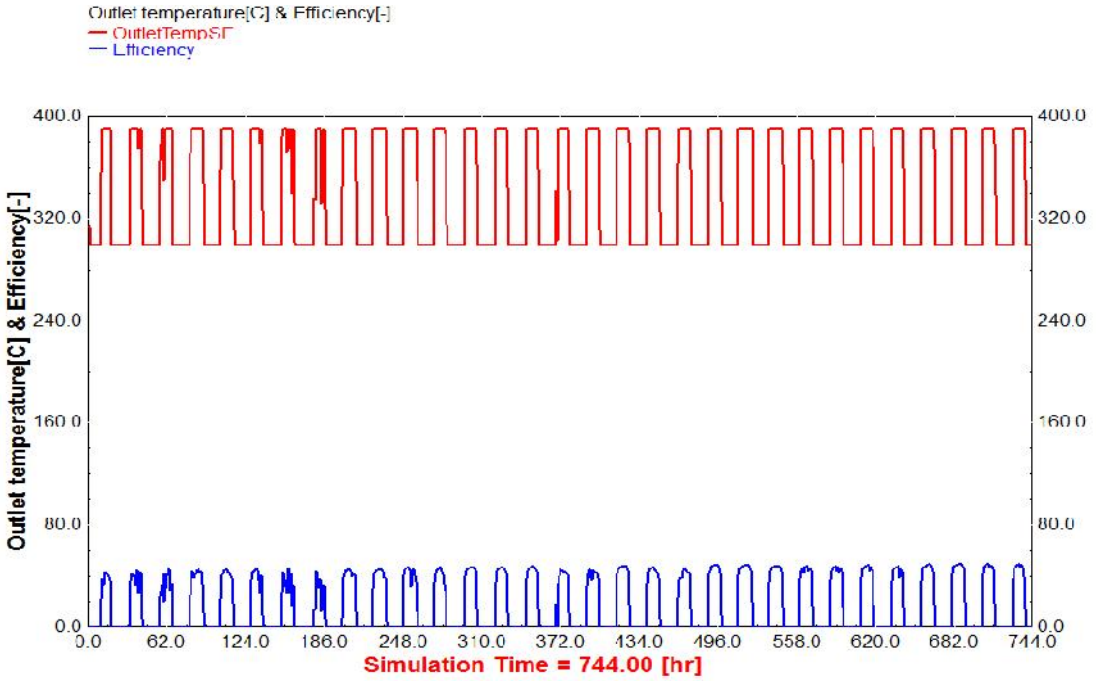

Figure 6.7: Daily output of outlet temperature and efficiency of solar field from January 1 to 30, 2001

Simulation for the intended power plant has been run. Due to the variation in DNI on different days for the given year has given result of varied power output. For representative date of January 23 and July 20, the DNI and power output are shown in Figure 6.8 to 6.13. Users easily can choose a time period and analyze performance in TRNSYS and get a Microsoft Excel output.

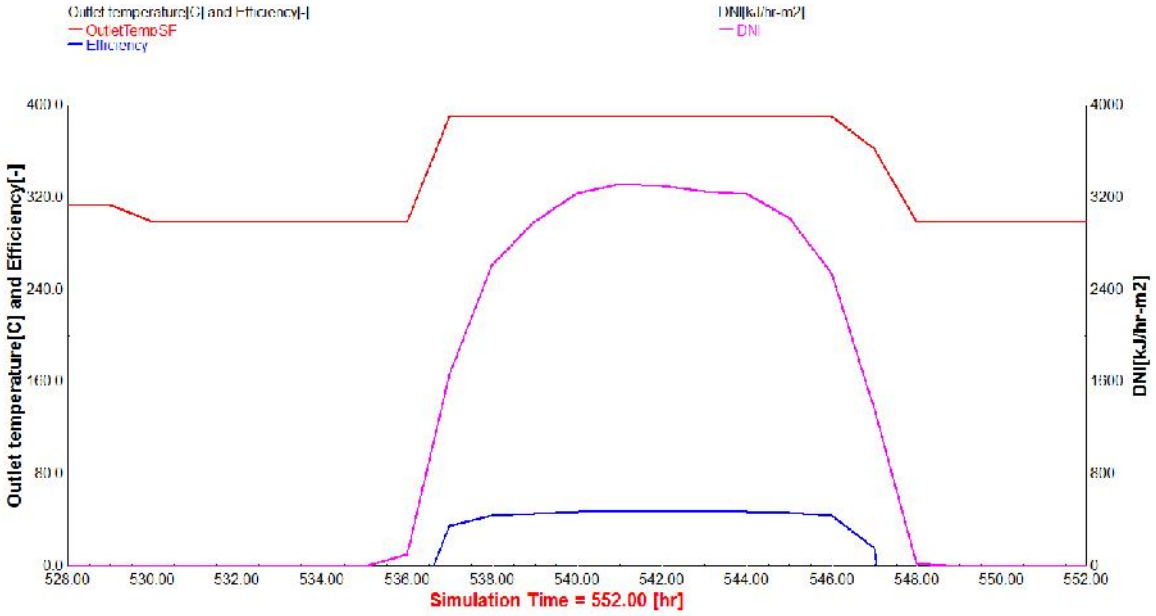

Figure 6.8: TRNSYS output of DNI, outlet temperature and efficiency of solar field for January 23

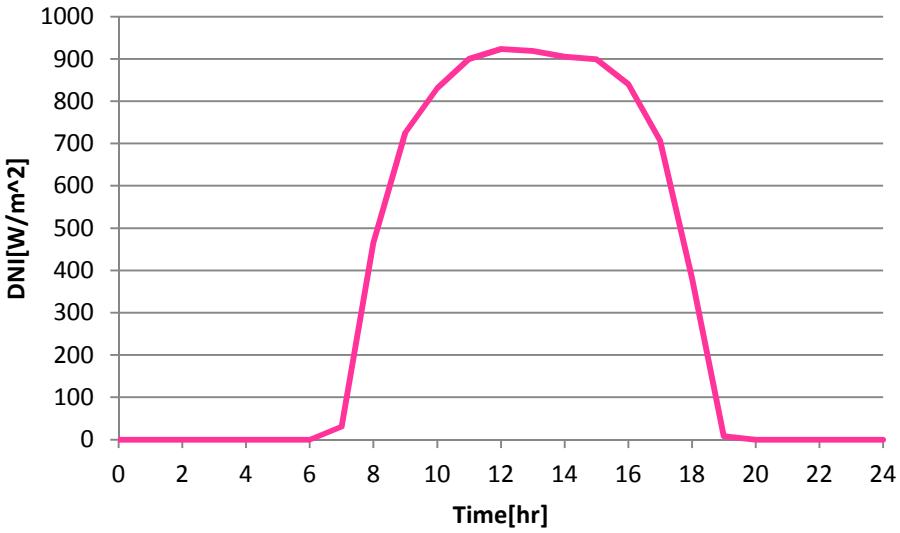

Figure 6.9: Direct Normal Irradiance for January 23, 2001

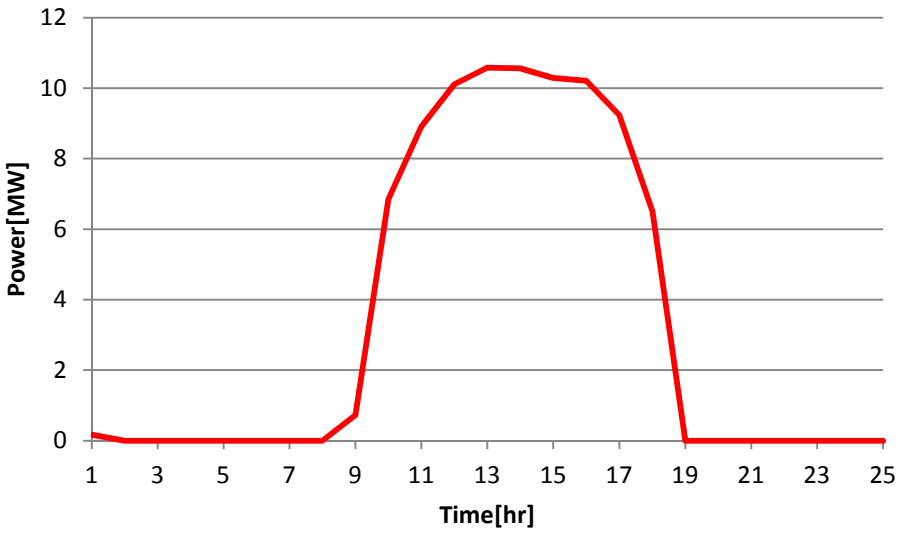

Figure 6.10: Power output for January 23, 2001

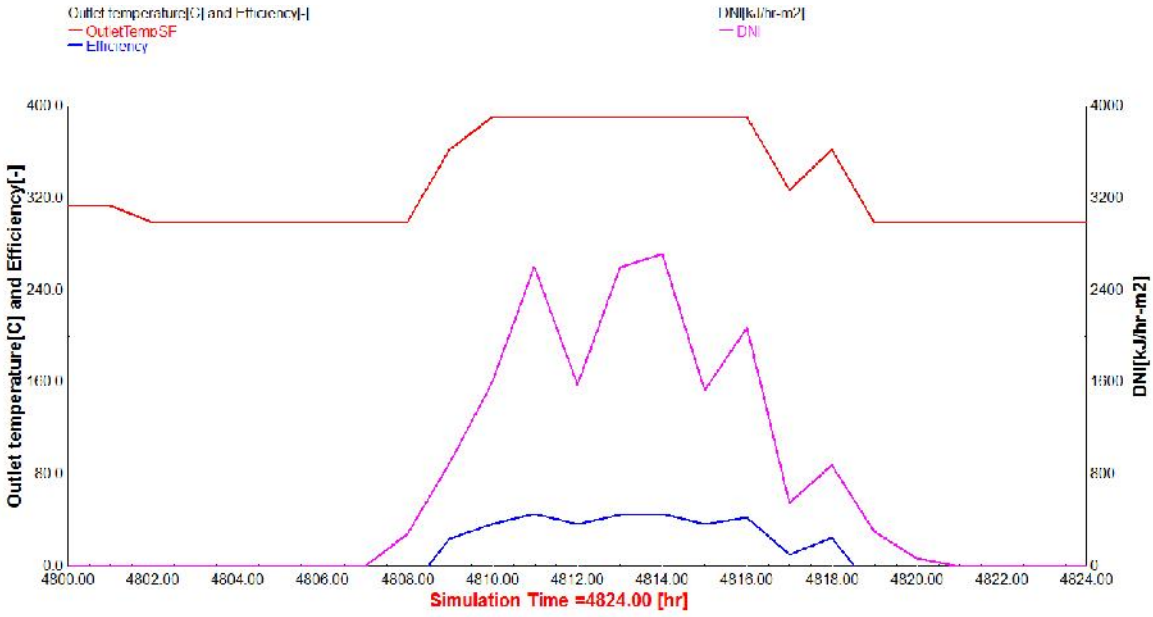

Figure 6.11: TRNSYS output of DNI, outlet temperature and efficiency of solar field for July 20

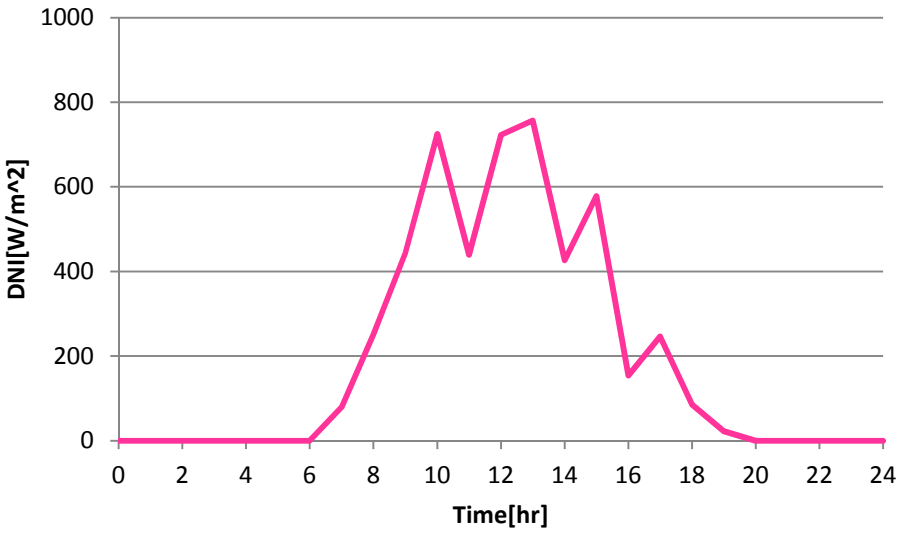

Figure 6.12: Direct Normal Irradiance for July 20, 2001

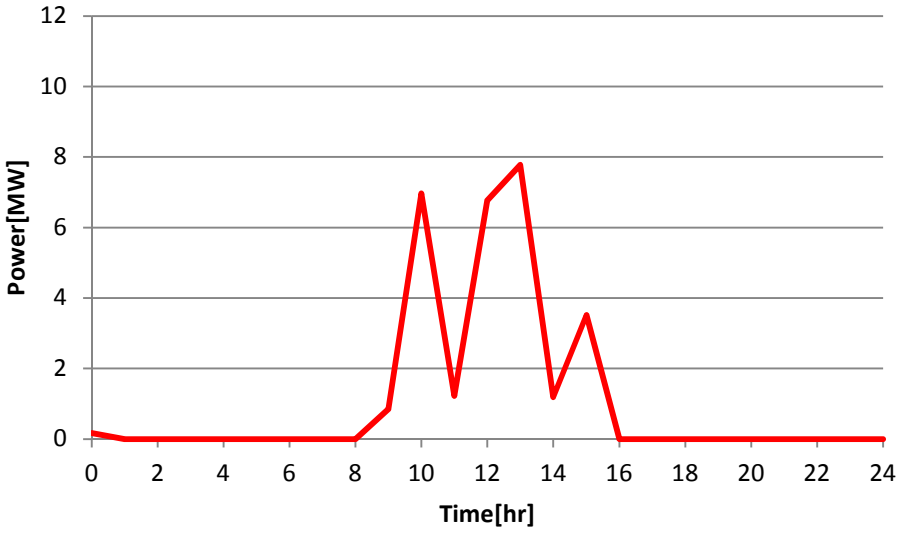

Figure 6.13: Power output for July 20, 2001

The simulation result of DNI and power output of other representative days of the year are shown in Appendix B.

Chapter 7: Cost of Electricity Generation of Parabolic Trough Plant

The System Advisor Model (SAM) is a performance and financial model designed to facilitate decision making for people involved in the renewable energy industry.

To perform simulation over a year, SAM software demands hourly data for which an EPW format weather data for the site is used.

7.1 Power Plant

The proposed plant has a capacity of 10MW. The plant consists of mainly solar field and power block. A heat transfer fluid (HTF) is heated as it circulates through the receivers in the solar field. It runs through the steam generator, which consists of multiple heat exchangers, to generate high-pressure steam. The HTF is then pumped back to the solar field. The generated steam is then fed into a separate cycle (Rankine cycle) to drive steam turbines. The discharged steam from the turbines is condensed into liquid ready to be heated in the steam generator to complete the cycle.

7.2 Solar Field

The proposed plant is occupied mostly by the solar field. The solar field consists of 348 LS-2 collectors divided on 29 loops (12 collectors per loop) with a total aperture area of 81,742 m^2.

The collected solar energy is converted into internal energy and transferred to the power cycle by the HTF which is distributed in the solar field through steel pipes with roughness of $4.5x10^{-5}$ m. The HTF called Therminol VP-1 is chosen as its thermal stability can be kept up to working temperatures of 400^oC. It has a wider liquid temperature range than water, but a lower thermal capacity and higher viscosity. It is a eutectic mixture of two very stable compounds, Biphenyl Oxide and Diphenyl.

Table 7.1: Characteristics of LS-2

Collector	LS-2
Aperture area [m^2]	235
Aperture width [m]	5
Length [m]	49
Receiver diameter [m]	0.07
Number of modules assembly	6
Optical efficiency	0.764
Receiver absorptivity	0.99
Mirror reflectivity	0.935

The Solar Field page displays variables and options that describe the size and properties of the solar field, properties of the heat transfer fluid. It also displays reference design specifications of the solar field.

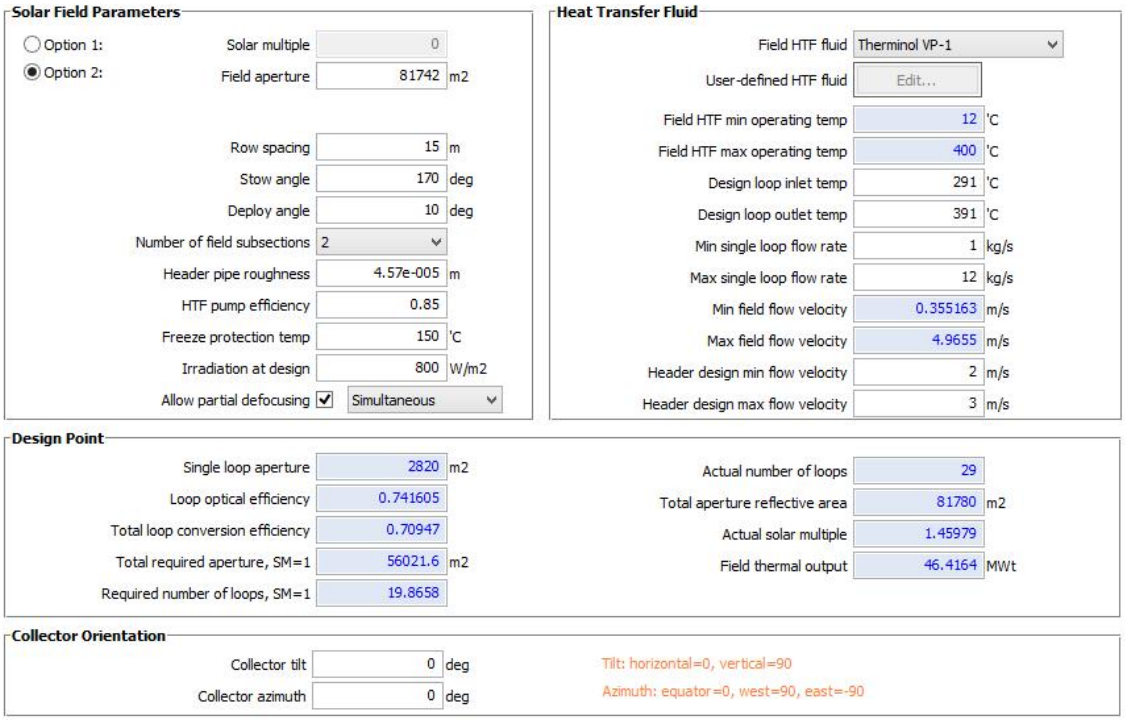

Figure 7.1: The solar field input page

7.3 Collector and Receiver (SCAs and HCEs)

On the collectors page, the characteristics of up to four collector types can be defined. LUZ LS-2 is chosen as the collector type from library. Depending on the chosen collector, the collector geometry is shown detailed in Figure 7.3.

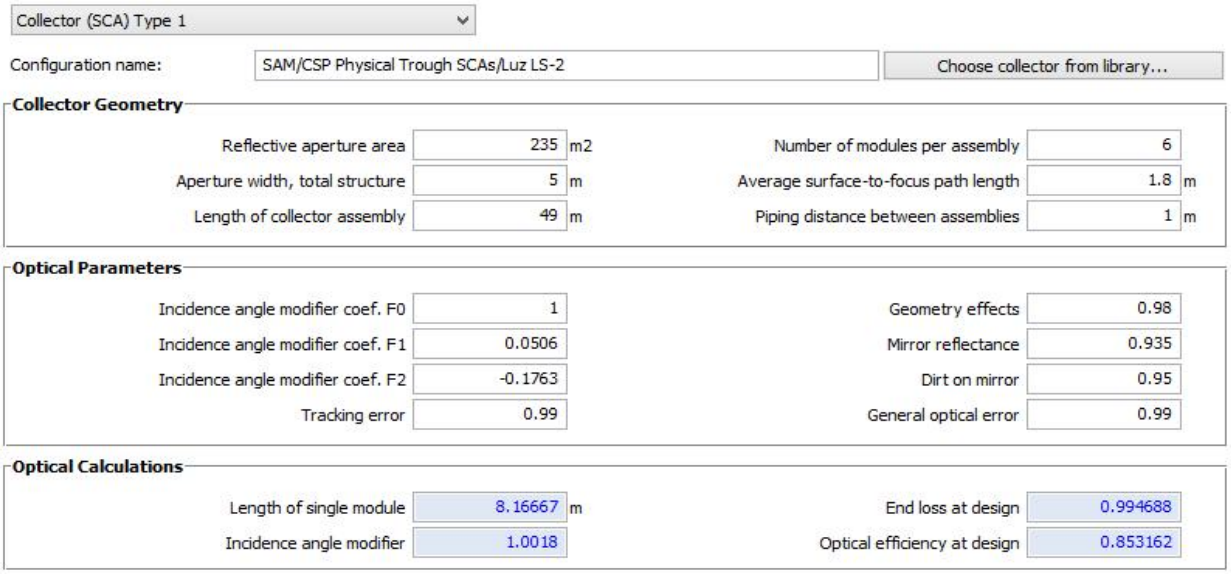

Figure 7.3: SCA input pages

A receiver (HCE, heat collection element) is a metal pipe contained in a vacuum within glass tube that runs through the focal line of the trough-shaped parabolic collector. On the Receivers page, the characteristics of up to four receiver types can be defined. Schott PTR70 2008 is chosen as a receiver from the library of available receivers.

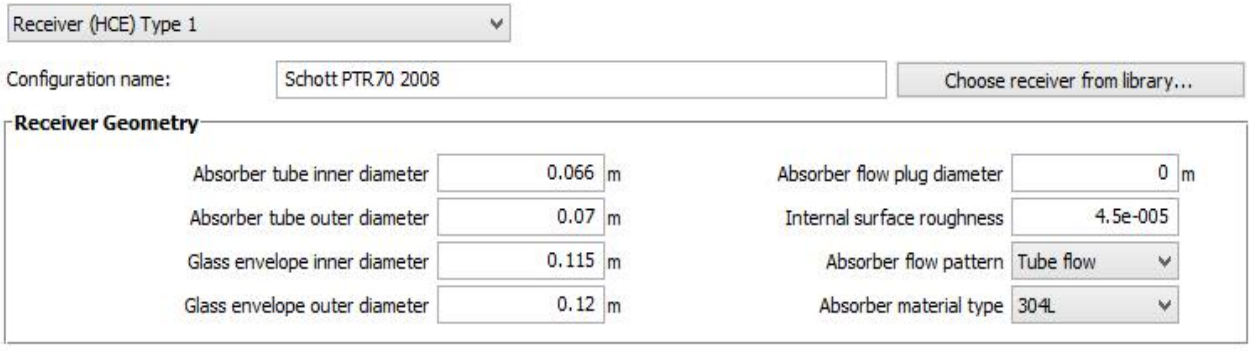

Figure 7.4: HCE input pages

7.4 Power Block

The power cycle model represents a power block that converts thermal energy delivered by the solar field and optional thermal energy system to electric energy using a conventional steam Rankine cycle power plant.

Capacity and operation parameters of the power cycle are as follows:

- Nominal Capacity: 10.0 MW.
- Conversion efficiency: 37.7%.

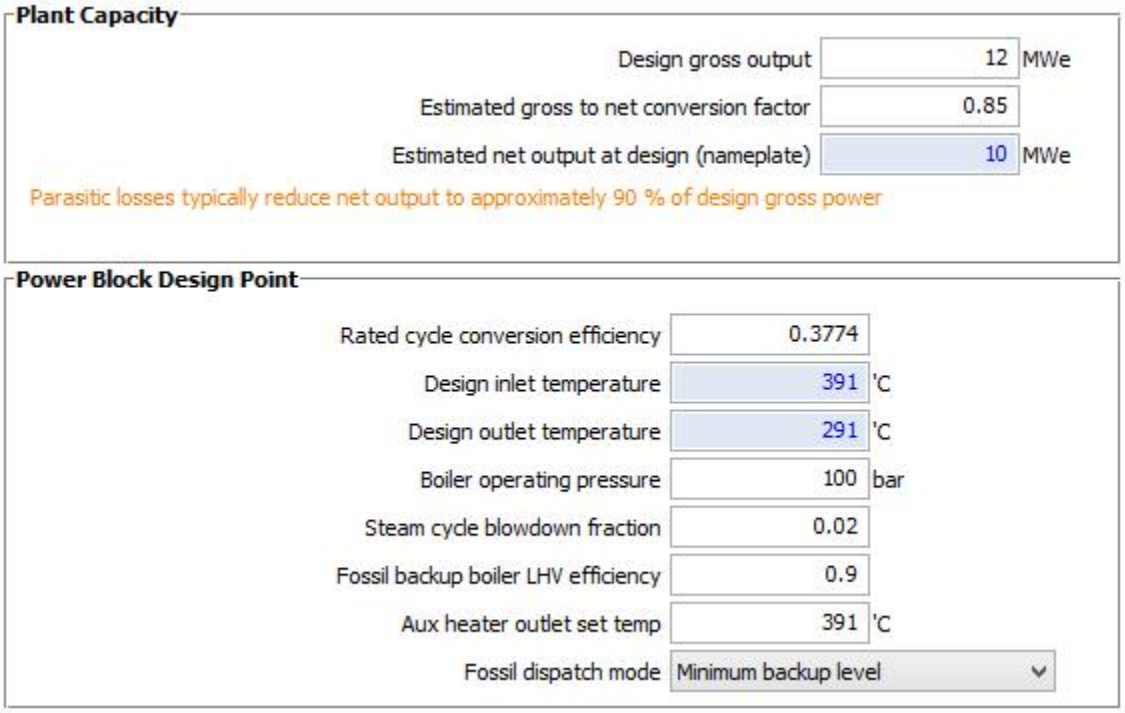

Figure 7.5: Power cycle page

7.5 Energy Yield Simulation

The System Advisor Model (SAM 2013.1.15) software provided by the (NREL) was used to estimate the energy yield of the parabolic trough plant. It was assumed that the plant will be unavailable for 4% of the operating time due to scheduled outages allocated basically for maintenance activities.

The simulation results are shown in Figures 7.6 and 7.7.It can be seen from Figure 7.6 that the maximum output power is realized in January as it has the maximum solar irradiation.

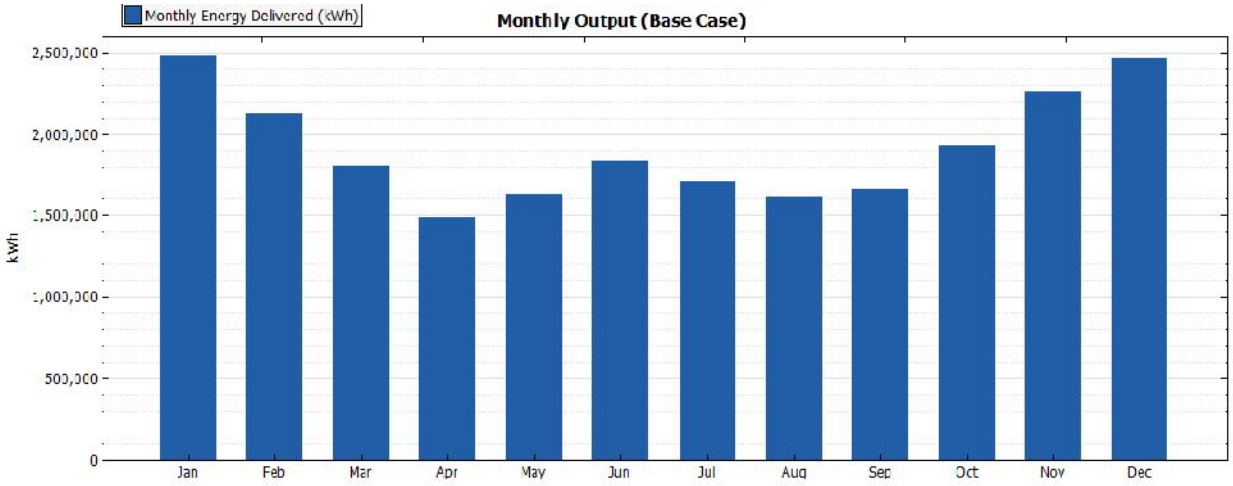

Figure 7.6: Monthly net electric output of the proposed plant.

Figure 7.7 provides a visual and numerical means for following the energy conversion through the complete electricity generation process.

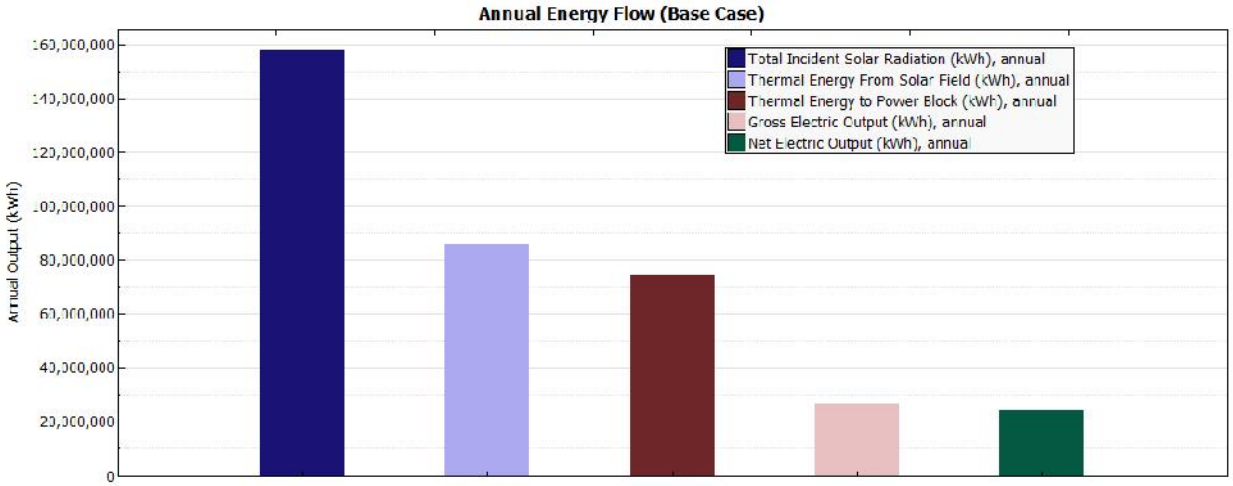

Figure 7.7: Annual energy flow through the proposed plant

The plant is expected to feed the national grid with 23,000 MWh of electric energy per year. This amount of energy is a result of converting 157,771 MWh of incident solar radiation by the

proposed plant achieving 14.6 % yearly conversion efficiency. The annual capacity factor of the plant can be calculated as:

Capacity factor = [Annual net energy output (MWh) / (10 MW x 8760 h)] x 100% = 26 %.

Other operational characteristics of the plant are summarized in Table 7.2

Table 7.2: Operational characteristics of the proposed plant

Total incident solar radiation [MWh/year]	157,771
Thermal energy from solar field [MWh/year]	85,595
Thermal energy from power block [MWh/year]	74,536
Gross electric output [MWh/year]	26,523
Net electric output [MWh/year]	23,000
Annual capacity factor [%]	26
Total annual conversion efficiency [%]	14.6

7.6 Economic and Financial Analysis

The financial analysis of the plant was performed using SAM software. This section introduces the results of the simulation related to the cost of electricity generation and the electricity price for the proposed plant. The simulation was executed for a base case scenario.

The analysis is a 20-year cash flow model for evaluating independent power producer (IPP) power plant project assuming that the electricity produced will be completely fed to the national grid at a price equal to the resulted LCOE (with no price escalation) through a power purchase agreement with the Ethiopian Electric Power Corporation (EEPCo.), the operator of the national grid.

7.6.1 Plant Costs

There are limited resources in the literature that provide cost breakdown for parabolic trough plants worldwide. In Addition, it was not possible to get the cost of the plant from local resources (contractors and suppliers) due to the lack of relevant experience. The most detailed

cost breakdown available from free resources is taken from sample file of Solar Advisor Model for 100 MW.

In order to estimate the capital cost of the proposed plant figures in conjunction with the following corrections and assumptions were applied.

- Contingency cost is 10 % of the total direct cost.
- The indirect costs (project development, management, procurement… etc) is 15% of the total direct cost.

The parabolic trough system cost used for the model has a total direct cost of $ 45,692,460 and indirect cost of $ 8,681,567. Hence the total installed costs $ 54,374,027.

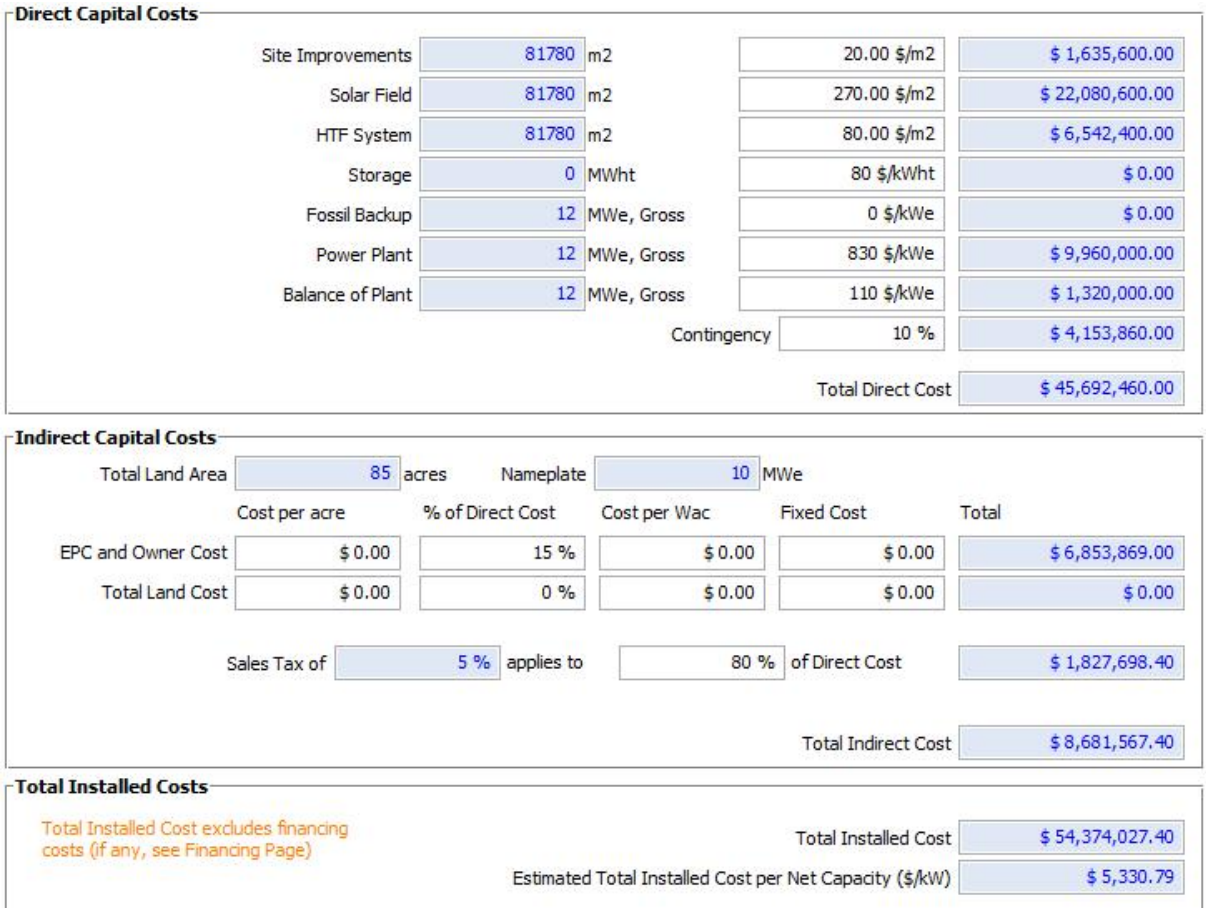

Direct Capital Costs

Site Improvements	81780	m2	20.00 $/m2	$ 1,635,600.00
Solar Field	81780	m2	270.00 $/m2	$ 22,080,600.00
HTF System	81780	m2	80.00 $/m2	$ 6,542,400.00
Storage	0	MWht	80 $/kWht	$ 0.00
Fossil Backup	12	MWe, Gross	0 $/kWe	$ 0.00
Power Plant	12	MWe, Gross	830 $/kWe	$ 9,960,000.00
Balance of Plant	12	MWe, Gross	110 $/kWe	$ 1,320,000.00
Contingency			10 %	$ 4,153,860.00
Total Direct Cost				$ 45,692,460.00

Indirect Capital Costs

Total Land Area: 85 acres — Nameplate: 10 MWe

	Cost per acre	% of Direct Cost	Cost per Wac	Fixed Cost	Total
EPC and Owner Cost	$ 0.00	15 %	$ 0.00	$ 0.00	$ 6,853,869.00
Total Land Cost	$ 0.00	0 %	$ 0.00	$ 0.00	$ 0.00

Sales Tax of 5 % applies to 80 % of Direct Cost: $ 1,827,698.40

Total Indirect Cost: $ 8,681,567.40

Total Installed Costs

Total Installed Cost excludes financing costs (if any, see Financing Page)

Total Installed Cost: $ 54,374,027.40

Estimated Total Installed Cost per Net Capacity ($/kW): $ 5,330.79

Figure 7.8: Cost page of the power plant model

7.6.2 Financial Parameters (Base Case Scenario)

The base case option displays variables for the base case results, which are results calculated using input values on the input pages. The base case scenario represents the anticipated financial terms for the investment in normal conditions with no incentives provided by the government.

Table 7.3: Financial parameters for the base case scenario

Parameter	Value	Remarks
Plant lifetime (investment period)	20 years	
Inflation rate (IR)	7.9%	This is the value of the inflation rate in Ethiopia for 2013.
Real discount rate (RDR)	6.00%	
Nominal discount rate (NDR)	14.37%	NDR account for the inflation rate according to the following formula: NDR = (1+RDR)(1+IR) - 1
Net salvage value	10.00%	Conservative assumption for the value of the plant at the end of the lifetime
Income tax rate	15.00%	% of the taxable income which equals to the operating income minus the debt interest payment
Insurance	0.30%	% of the total capital cost
Dept fraction	70.00%	% of the total capital cost to be borrowed
Loan term	20 years	
Loan rate	6.00%	Interest rate for commercial loan
Minimum required Internal Rate of Return (IRR)	12.00%	The minimum required rate of return on the equity for the investors.
Plant availability	96.00%	The plant is assumed to be out of operation for forced and scheduled maintenance activities for 4% of the operating hours

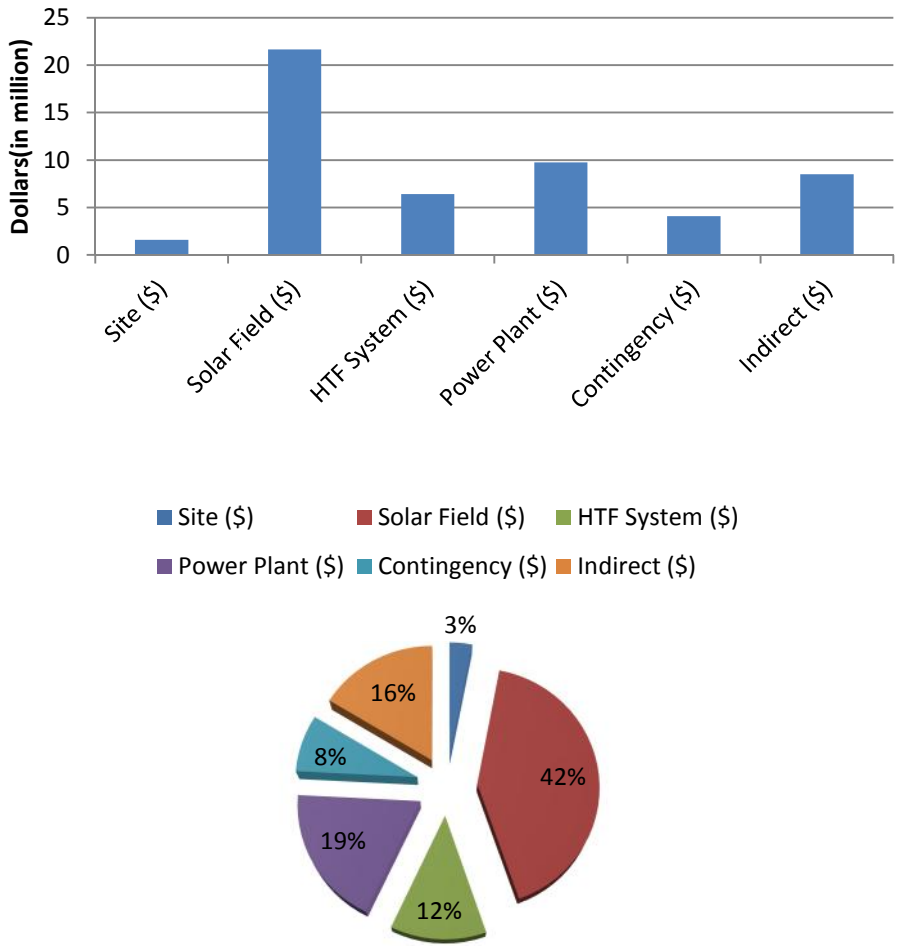

Figure 7.9: Share of the plant items in the total capital cost per watt and in percent

Table 7.4: Cost values for the 10 MW power plant **

Cost type	Value ($)
Site	1,635,600
Solar Field	22,080,600
HTF System	6,542,400
Power Plant	9,960,000
Contingency	4,153,860
Indirect	8,681,567

***The estimates of these costs are taken from sample file Solar Advisor Model for 100MW.*

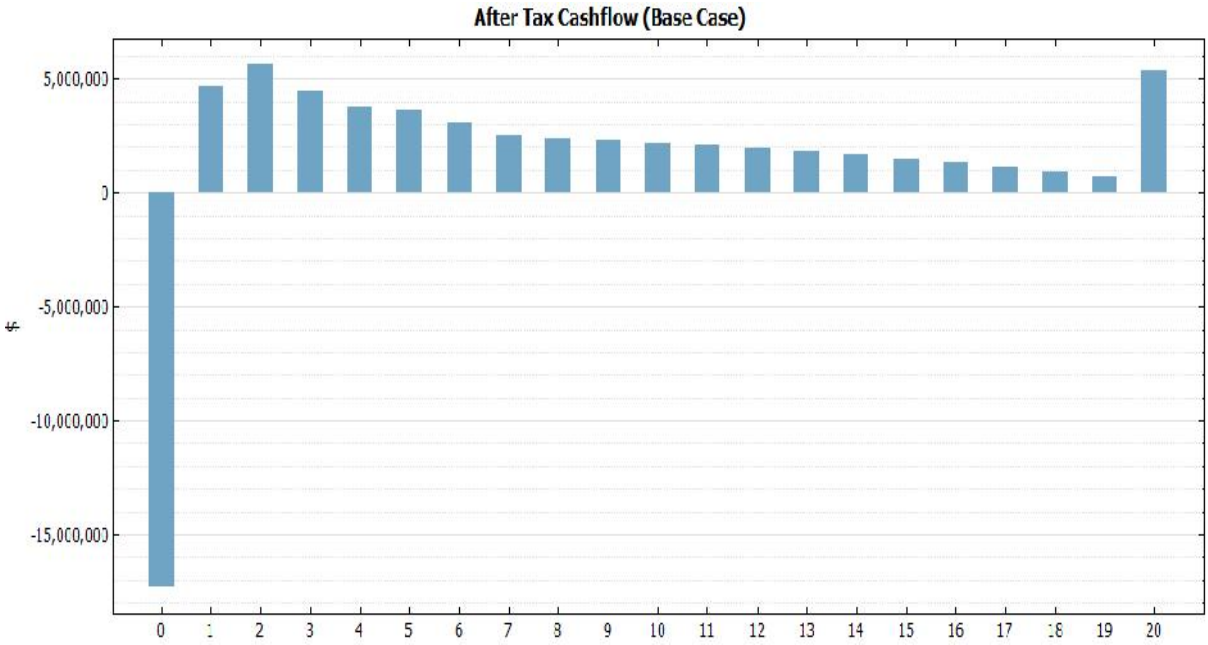

Figure 7.10: After-tax cash flow for the base case scenario

Table 7.5: After tax net equity cash flow ($) million

Year	After tax net equity cash flow ($)		Year	After tax net equity cash flow ($)
0	-17,290,900		11	2,066,280
1	4,666,270		12	1,938,700
2	5,642,480		13	1,801,370
3	4,469,950		14	1,653,560
4	3,735,070		15	1,494,440
5	3,658,770		16	1,323,160
6	3,078,690		17	1,138,770
7	2,492,350		18	940,256
8	2,397,270		19	726,539
9	2,294,940		20	5,395,540
10	2,184,810			

Table 7.6: Monthly energy flow

Month	Monthly Energy Delivered [kWh]	Solar Field Thermal Output [MWh]	Thermal Energy Absorbed by HTF [MWh]	Total Incident Thermal Energy [MWh]	Gross Electric Output [kWh]	Net Electric Output [kWh]
Jan	2,480,400.00	8,829.43	9,004.37	18,540.30	2,816,370.00	2,583,750.00
Feb	2,126,460.00	7,898.00	8,089.24	15,557.30	2,421,540.00	2,215,060.00
Mar	1,801,360.00	6,803.83	7,103.75	12,580.40	2,091,130.00	1,876,410.00
Apr	1,489,630.00	5,537.67	5,819.25	9,990.74	1,747,450.00	1,551,700.00
May	1,633,820.00	5,852.51	6,127.78	10,552.60	1,906,330.00	1,701,900.00
Jun	1,836,550.00	6,313.99	6,548.30	11,310.70	2,117,030.00	1,913,080.00
Jul	1,712,710.00	5,948.00	6,158.29	10,615.10	1,991,150.00	1,784,070.00
Aug	1,613,260.00	5,732.58	5,945.47	10,039.10	1,892,560.00	1,680,480.00
Sep	1,657,710.00	5,916.22	6,155.80	10,352.10	1,932,130.00	1,726,780.00
Oct	1,928,340.00	6,957.14	7,361.80	13,272.20	2,223,050.00	2,008,680.00
Nov	2,263,500.00	7,904.20	8,368.18	16,347.40	2,577,120.00	2,357,810.00
Dec	2,463,350.00	8,585.76	8,913.20	18,612.90	2,807,950.00	2,565,990.00

The financial simulation resulted in an LCOE of 19.49 ¢/kWh which is still high when compared to the current cost of electricity in Ethiopia (0.017 ¢/kWh) which is being generated mostly by hydropower plant. However, taking of energy mix into consideration, parabolic trough plants can highly contribute to the energy security in Ethiopia as well as to neighboring countries which buys power from Ethiopia where power generating resources are extremely limited.

Chapter 8: Conclusion and Recommendation

8.1 Conclusion

In this study, a model for the solar field and power cycle was created in the TRNSYS simulation environment using the Solar Thermal Electric Component (STEC) model library. A model for a 10 MW CSP system was developed based on an actual 30 MW system in Kramer Junction, California. The system consists of a collector loop connected to a power block by a series of heat exchangers. The collector loop consists of a field of parabolic trough collectors, expansion vessel, pump and heat exchangers to drive the power block and uses a heat transfer fluid. The series of heat exchangers connecting the collector loop to the power block are a preheater, steam generator, superheater, and reheater. In addition to these heat exchangers, the power block for the 10 MW consists of a 2-stage high pressure turbine, 3-stage low pressure turbine, condenser, 3-feed water heaters, a deaerator, and 2-pumps reducing two low pressure turbines and feed water heaters from the 30 MW model.

The performance of the model developed in the TRNSYS is evaluated for year 2001. The power output, DNI, efficiency and solar field outlet temperature of January 23 and July 20 for selected year are plotted using TRNSYS and Microsoft Excel output. The results of the simulation have shown that power produced is heavily dependent on DNI. This can be seen from power graph preserved the shape of the DNI graph.

Cost and financial analyses are made for this power plant using Solar Advisor Model (SAM). The analysis is made by modeling the power plant with a specified capacity under Adigala weather condition. The results of this model give for net turbine capacity of 10 MW a total installed cost of $ 54,374,027. From which 42 % of this total installed cost is the solar field, being the major source of cost ($ 22,080,600).

The annual energy output from the plant was estimated to be 23,000 MWh achieving a yearly conversion efficiency of 14.6 %. The financial simulation resulted in an LCOE of 19.49 ¢/kWh which is still high when compared to the current cost of electricity in Ethiopia (0.017 ¢/kWh) which is being generated mostly by hydropower plants. However, taking energy mix into consideration, parabolic trough plants can highly contribute to the energy security in Ethiopia.

8.2 Recommendation

This presented study forms a foundation and should be considered as a starting point for further studies. It is a basic development for a very promising technology which is the parabolic trough collector system. In the future with required developments and research, these systems can be more commercially viable. Suggestions to improve on this present modeling and simulation work are as follows:

- The current model does not include storage. Storage can be implemented to improve the availability of this system and shift electricity production closer to peak electricity demand.
- The current model only includes Therminol VP-1 as a heat transfer fluid. These models can be improved by implementing water instead of Therminol VP-1 to model a direct steam generation (DSG) system. As a result, some new important aspects, such as collector efficiency can be introduced.
- Parabolic trough plants are capital-intensive projects and cost reduction should be investigated and improved.

Reference

[1] IPCC, 2007a---Intergovernmental Panel on Climate Change (2007): Climate Change 2007 Synthesis Report Summary for Policymakers. Geneva: Intergovernmental Panel on Climate Change (IPCC)

[2] Minister of Water and Energy, Energy Balance and Statistics for years 2005/6-2009/10, August 25, 2011.

[3] Ministry of Water and Energy, April 15-04-2011, Ethiopian Energy Potential And Five Year Energy Sector GTP

[4] NASA Surface meteorology and Solar Energy – Location

[5] Assessment of the world bank/GEF strategy for the market development of concentrating solar thermal power

[6] M. Ragheb (2011). Solar Thermal Power and Energy Storage Historical Perspective

[7] Solar Parabolic Trough. Energy Technology Network, Solar Paces website Retrieved September 27, 2012 from http://www.solarpaces.org/CSP_Technology/docs/solar_trough.pdf

[8] Solar Parabolic Trough. Energy Technology Network, Solar Paces website Retrieved September 27, 2012 from http://www.solarpaces.org/CSP_Technology/docs/ solar_trough .pdf

[9] National Renewable Energy Laboratories. Retrieved September 12, 2012 from http://www.nrel.gov/csp/solarpaces/by_technology.cfm

[10] Lippke, F., 1995. Simulation of the part-load behavior of a 30MWe SEGS plant. Tech.rep., SAND–95-1293, Sandia National Labs., Albuquerque, NM (United States)

[11] Jones, S., Pitz-Paal, R., Schwarzboezl, P., Hohe, L., Blair, N., and Cable, R., 2001. “TRNSYS Modeling of the SEGS VI Parabolic Trough Solar Electric Generating System”. In Proceedings of Solar Forum 2001: Solar Energy: The Power to Choose, Washington, DC, USA, p. 405

[12] Quaschning, V., Kistner, R., and Ortmanns, W., 2002. “Influence of direct normal irradiance variation on the optimal parabolic trough field size: A problem solved with technical and economical simulations”. Journal of Solar Energy Engineering, 124, pp. 160–164

[13] Patnode, A. M. “Simulation and performance evaluation of parabolic trough solar power plants”. Master’s thesis, University of Wisconsin-Madison., College of Engineering, 2006

[14] [IPCC, SREEN] [IPCC, SREEN]: Edenhofer, O / Madruga, R / Sokona, Y (2012): Renewable Energy Sources and Climate Change Mitigation. Special Report of the Intergovernmental Panel on Climate Change. Cambridge: University Press.

[15] Jensen, C., Price, H., and Kearney, D., “The SEGS Power Plants: 1988 Performance”, 1989 ASME International Solar Energy Conference, San Diego, CA, April 1989

[16] Jones, Scott A., Pitz-Paal, R., Schwarzboezl, P., Blair, N., and Cable, R. "TRNSYS Modeling of the SEGS VI Parabolic Trough Solar Electric Generating System ", Proceedings of Solar Forum 2001, Washington, D.C. April 2001.

[17] El-Wakil, M. M. Power plant Technology. New York: McGraw-Hill, Inc., 1984.

Appendixes

Appendix A

Calculations Used to Find State Reference Points in MATLAB [13]

Turbine pressure optimization

The optimum pressure at which the feedwaters are to be placed is obtained by finding the temperature difference that would divide the temperature difference between the boiler (saturation temperature of the boiler) and the condenser temperature into equal parts that are equivalent to the number of feedwater heaters [17].

$$\Delta T_{opt} = \frac{T_b - T_c}{n+1} \qquad A-1$$

where: ΔT_{opt} = Temperature rise between feedwaters

T_b= the saturated temperature of the boiler

T_c=the condenser temperature, and

n=the number of feedwater heaters

The entropy at the section inlet is calculated from the inlet pressure and enthalpy:

$$s_{inlet} = s(P_{inlet}, h_{inlet}) \qquad A-2$$

The isentropic enthalpy at the section outlet is calculated from the outlet pressure and entropy at the section inlet:

$$h_{outlet,s} = h(P_{outlet}, s_{inlet}) \qquad A-3$$

The temperatures of the streams are evaluated from the pressures and enthalpies at the desired state.

$$T_{inlet} = T(h_{inlet}, P_{inlet}) \qquad A-4$$

The reference efficiency of the section is defined as the ratio of the actual change in enthalpy to the isentropic change in enthalpy:

$$\eta = \frac{h_{steam,in} - h_{steam,out}}{h_{steam,in} - h_{steam,out}, s} \qquad A-5$$

UA: Closed Feedwater Heaters

There are three closed feedwater heaters in the 10 MW power cycle, one of which utilize steam extracted from the low pressure turbine (FWH1) and two of which use extractions from the high pressure turbine (FWH2 and FWH3 ; Deaerator is the open feedwater heater). All feedwater heaters are supplied with feed water on the tube side of the heat exchanger. FWH3 and deaerator run only extracted steam through the shell side, whereas FWH2 and FWH1 run a mixture of extracted steam and drain water cascaded back from next highest feedwater heater(s) in the series.

The exit enthalpy of the condensed steam (condensate) is that of saturated liquid at the inlet pressure to the feedwater heater, assuming that no pressure drop occurs over the condensing steam:

$$P_{steam,in} = P_{steam,out} \qquad A-6$$

The heat transfer between streams may be calculated from the change in enthalpy of the steam.

$$\dot{Q}_{water} = \dot{m}_{steam} C_{pwater,in} \left(T_{water,out} - T_{water,in}\right) \qquad A-7$$

But this heat transfer rates are equal for ideal cases. In the above equation the specific heat capacity of the inlet water is calculated at the given water temperature and pressure.

$$C_{pwater,in} = C_p \left(T_{water,in}, P_{water,in}\right) \qquad A-8$$

The maximum heat transfer is determined from the capacitance rate of the feedwater multiplied by the difference in temperature between the two inlet streams:

$$\dot{Q}_{max} = \dot{m}_{water} \cdot \dot{c}_{water} \left(T_{in,steam} - T_{water,in}\right) \qquad A-9$$

The ratio of actual heat transfer to maximum heat transfer establishes the reference effectiveness of the heat exchanger.

$$\varepsilon_{water} = \frac{\dot{Q}_{water}}{\dot{Q}_{max}} \qquad A-10$$

For heat exchangers in which one fluid undergoes a phase change, the effectiveness is related to the number of transfer units (NTU) through the following equation:

$$\varepsilon_{water} = 1 - \exp(-NTU_{water}) \qquad A-11$$

Finally, the ratio of the NTU to the heat capacitance of the feed water equals the reference UA of the heat exchanger:

$$NTU_{water} = \frac{UA_{water}}{\dot{m}_{water} C_{pwater}} \qquad A-12$$

The temperatures of the feedwaters are evaluated from the pressures and enthalpies using property relation for water

$$T_{feadwater,out} = \mathrm{T}\,(P_{feedwater,out}, h_{feedwater,out}) \qquad A-13$$

UA: Heat Exchangers

The specific heat for each fluid is evaluated from the difference in enthalpy of the inlet and exit, divided by the temperature difference between inlet and exit.

$$C_{psteam} = \frac{h_{steam,out} - h_{steam,in}}{T_{steam,out} - T_{steam,in}} \qquad A-14$$

$$C_{pHTF} = \frac{h_{HTF,out} - h_{HTF,in}}{T_{HTF,out} - T_{HTF,in}} \qquad A-15$$

The capacitance rate of each stream is the product of its mass flow rate and specific heat:

$$C_C = \dot{m}_{steam} C_{psteam} \qquad A-16$$

$$C_H = \dot{m}_{HTF} C_{pHTF} \qquad A-17$$

The minimum and maximum heat capacitance rates of the two streams are identified, and the capacitance rate ratio is calculated:

$$C_{min} = MIN(C_c, C_H) \qquad A-18$$

$$C_{max} = MAX(C_c, C_H) \qquad A-19$$

$$C_r = \frac{C_{min}}{C_{max}} \qquad A-20$$

The maximum heat transfer is determined from the smaller capacitance rate of the two fluids multiplied by the difference in temperature between the two inlet streams:

$$\dot{Q}_{max} = C_{min}\left(T_{in,HTF} - T_{in,steam}\right) \qquad A-21$$

The ratio of actual heat transfer to maximum heat transfer establishes the reference effectiveness of the heat exchanger. The reference effectiveness is calculated both using the heat transfer calculated on the steam side and using the heat transfer calculated on the heat transfer fluid side.

$$\varepsilon = \frac{\dot{Q}}{\dot{Q}_{max}} \qquad A-22$$

For counter flow heat exchangers, the effectiveness is related to the number of transfer units (NTU) and capacitance ratio through the following equation:

$$\varepsilon = \frac{1 - \exp\left[-NTU.(1 - C_r)\right]}{1 - C_r \exp\left[-NTU.(1 - C_r)\right]} \qquad A-23$$

The ratio of the NTU to the heat capacitance of the feed water equals the reference UA of the heat exchanger:

$$NTU = \frac{UA}{C_{min}} \qquad A-24$$

Appendix B

B.1 Simulation result for April 24

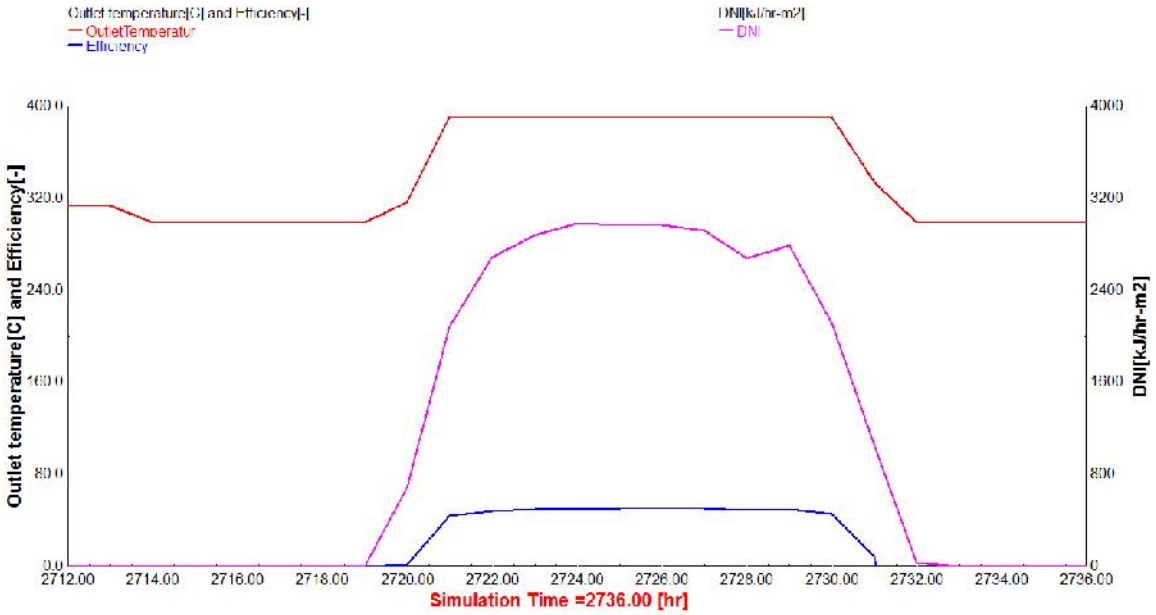

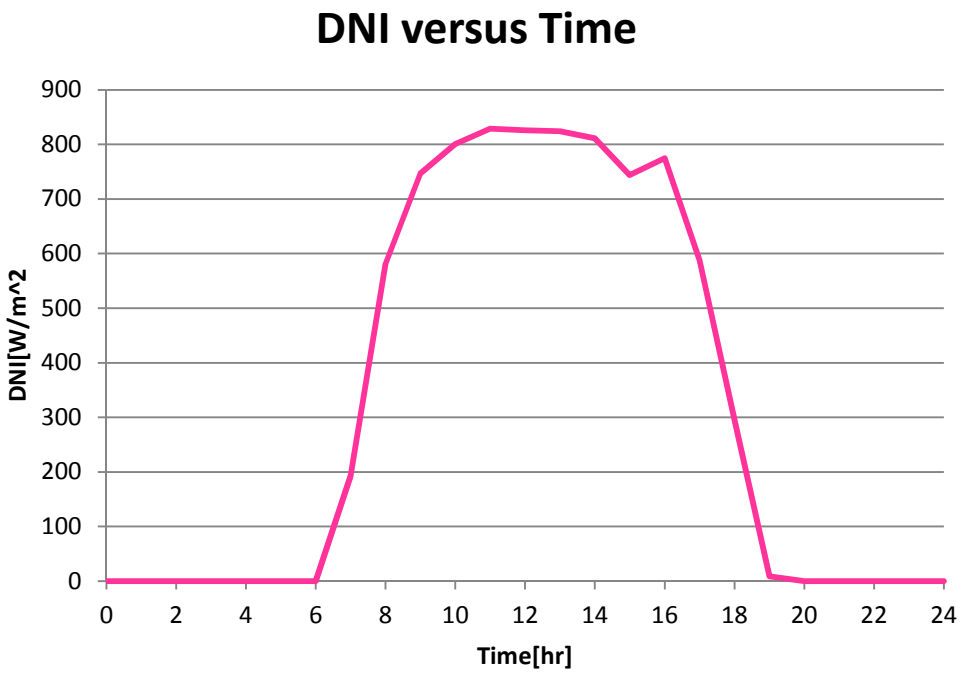

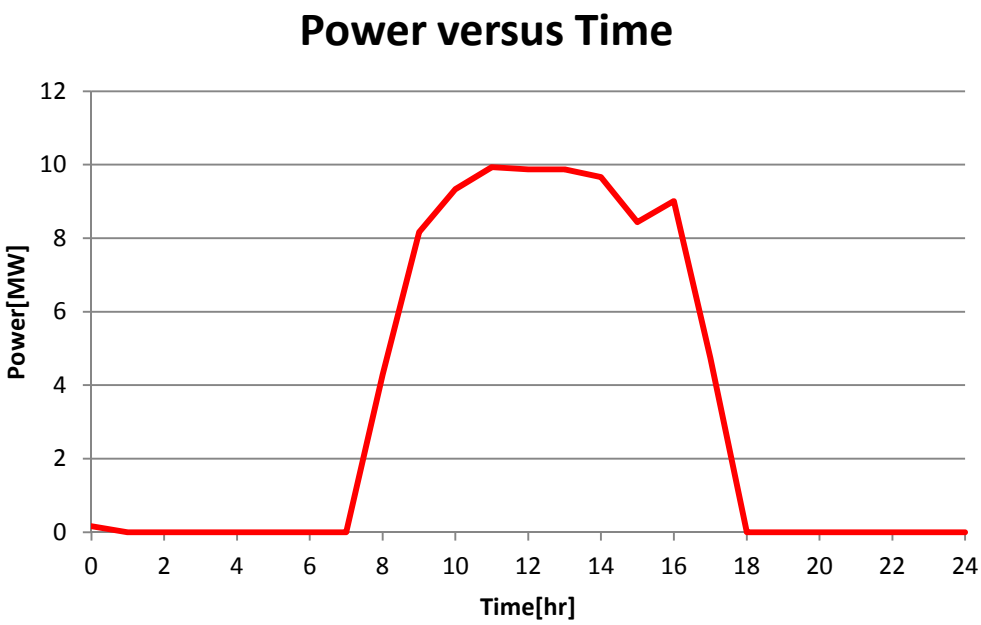

B.2 Simulation results for November 9

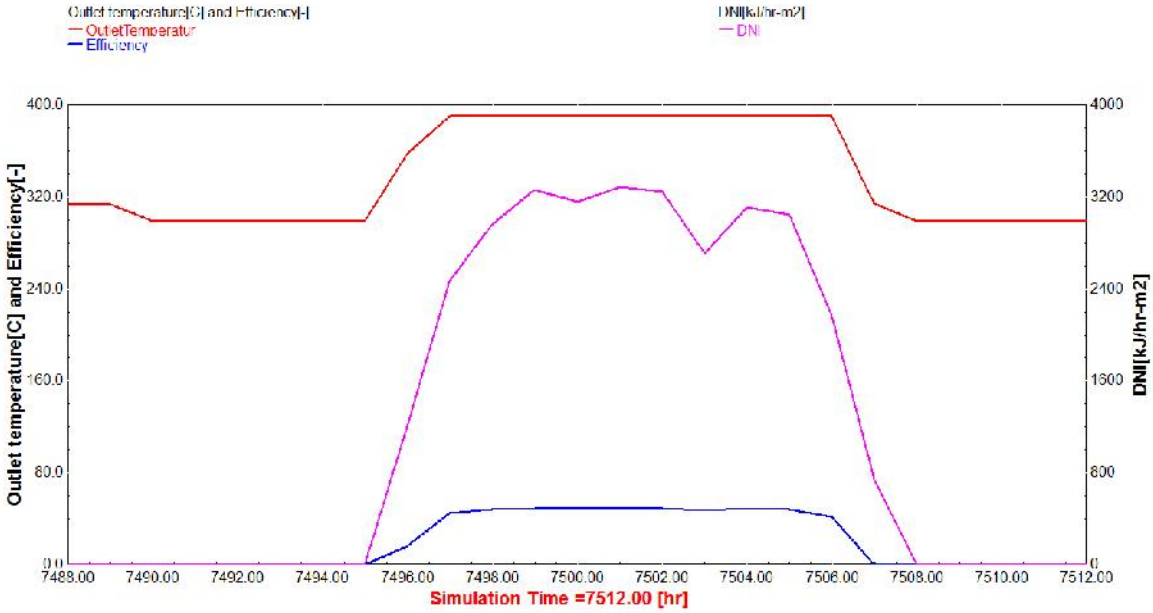

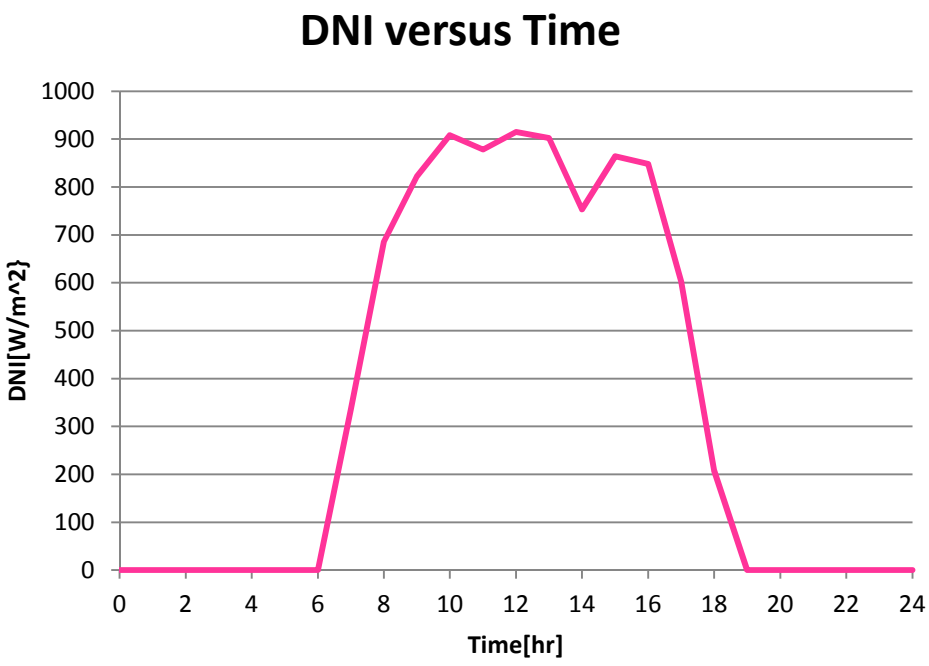
DNI versus Time
DNI[W/m^2}
1000
900
800
700
600
500
400
300
200
100
0
0 2 4 6 8 10 12 14 16 18 20 22 24
Time[hr]

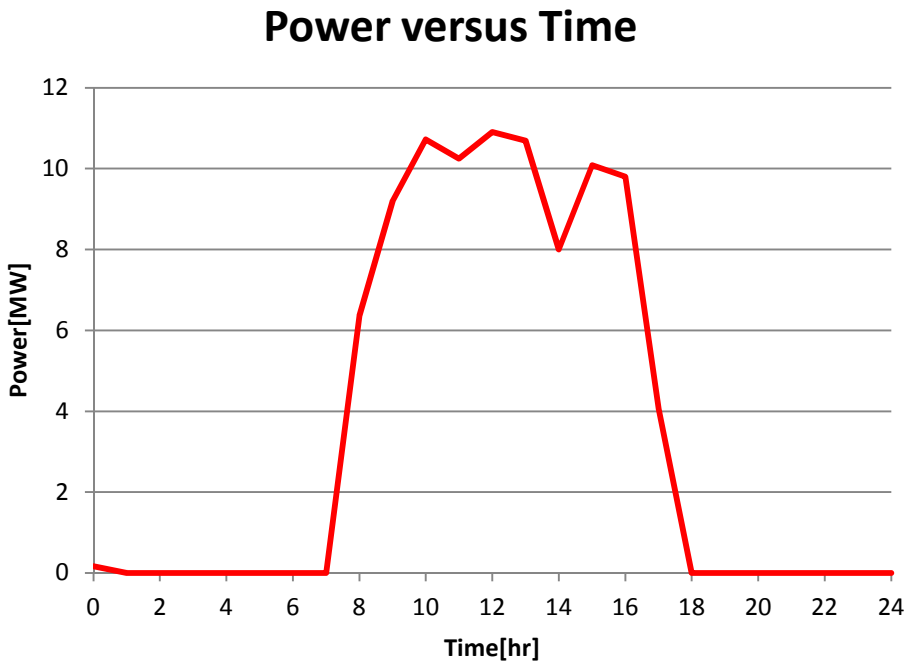
Power versus Time
Power[MW]
12
10
8
6
4
2
0
0 2 4 6 8 10 12 14 16 18 20 22 24
Time[hr]